

I would like to thank Prof. Ramiro Neves for welcoming me into the MARETEC – group and the suggestion of an interesting research subject & my tutor, Mr. Guillaume Rifflet for his patience & his guidance in this work.

Table of contents

| | |
|--------------------------|------|
| Table of contents | p.1 |
| I Introduction | p.4 |
| II Review of literature | p.14 |
| III Data & methods | p.25 |
| IV Validation of results | p.34 |
| V Results | p.43 |
| List of figures | p.45 |
| References | p.47 |
| Electronic appendix | |

I Introduction

The northeastern Atlantic Ocean west off the Iberian Peninsula is an extremely interesting region from oceanographic point of view. The Iberian system is marked by a strong seasonal variability which is mainly due to the displacement of the Azores High. In summer, the Azores High migrates north and induces southward surface currents. These favorable upwelling conditions occur between April and October (Fíuza & al., 1982). In winter, the Azores high migrates back south and poleward currents can be found at all levels in the water column.

The water column is constituted of surface, intermediate and deep waters which are all clearly distinguishable by their respective differences in potential temperature and salinity. The surface layer contains both surface and central waters. These central waters consist of fresher waters of subtropical origin (ENACW_{st}) overlying denser and slightly cooler central waters (ENACW_{sp}) of subpolar origin. At the intermediate level Mediterranean waters (MW) become dominant. These Mediterranean waters are subjected to a lot of topographical steering as they enter the Atlantic Ocean through the Strait of Gibraltar. Because the Iberian continental shelf is seeded with topographical features such as capes, promontories and submarine canyons with spatial scales of tens to hundreds of kilometers, the Mediterranean Outflow experiences a lot of mixing with surrounding water masses. In the northwestern part of the region, below 1400m of depth, some Labrador Sea Water can be found. Deep waters are marked by a mixed layer of MW, LSW (in some regions) and NADW (North Atlantic Central Water) which overlies a vast, homogenous layer of NADW. The physical characteristics of these water masses and their circulation are elaborately discussed in chapter II (Fíuza & al., 1998).

These water masses do not only experience seasonal changes, they are also subjected to a lot of submesoscale processes like jets, meanders, eddies, upwelling filaments and countercurrents. These submesoscale features have a timescale of a few tens of days and are superimposed to the seasonal variations. They have a profound influence on water masses offshore and on the continental shelf and constitute the ocean's response to sub-seasonal timescales and sub – basin spatial scales. Consequently, they dominate the ecosystem off the Western Iberian Peninsula (Relvas & al., 2007).

In this study we will use the MOHID – model of the Instituto Superior Técnico to simulate ocean dynamics on monthly timescales in the region between -12.67 and 5.53°W and 34.3 and 45.03°N for the period from June 1st, 2006 until June, 26th 2007. The aim of this simulation is to obtain a better understanding of the seasonal variability of the physical oceanography of the upper water layers off the Western Iberian Peninsula, to identify the different water masses implicated in these processes and to quantify the fluxes of different water masses. In order to do so, the model will provide us with two daily fields of temperature and salinity and with monthly residual velocity. In order to quantify the transports of the different water masses we introduced a new spatial discretisation into the model. Horizontally we defined 42 boxes in function of the bathymetry of the region. Vertically, 43 layers varied exponentially between indicator depths for the interfaces between main water masses. These indicator depths were subsequently used to define 7 vertical boxes that re – group the vertical layers.

Besides this spatial discretisation, we also provided the model with a bathymetry, initial and boundary values for temperature, salinity and velocity, main river discharges and meteorological and tidal data. The model will introduce these data into a semi – implicit ADI - scheme¹ to discretise in time and into a TVD – superbee scheme to discretise in space. Initial conditions for temperature and salinity are provided by the Mercator – model while initial velocities are zero. Once these discretised equations are solved, the model will apply boundary conditions and a sponge layer in the ten outmost grid cells.

The output of the model consists of 12 – hourly files for water properties and velocities and of 24 – daily volume fluxes through the pre – defined boxes. These data are then validated in order to gain a better understanding of the nature of the model’s biases. As there are only very few in situ data, the model is first compared to an annual climatology and to the Mercator – model. These comparisons already show that the nature of most errors is due to different initial or boundary conditions or to the use of different bathymetries. Then the model is compared to the in situ data of the MORENA – campaign (1993) which confirms us that the model provides us with a fairly good representation of the different water masses. Finally, the model is also compared to the in situ data of Argo – floaters. We found that the MOHID – data is slightly less saline in the 2006 surface waters and in intermediate waters. The 2006 salinity bias is due to the poor temporal resolution of meteorological data, whereas the origin of the error in salinity in intermediate water is probably due to exaggerated vertical diffusion by the model.

As validation confirms the quality of our data, we shall finally start to analyze the generated volume fluxes. Since there is only very little data to compare these fluxes to, we shall compare them with monthly mean fields of temperature, salinity and velocity in order to identify the circulation of different water masses and quantify them. Because these residual volume fluxes are only generated once every 24 days, we shall have to use other data to identify sub - mesoscale features with a shorter time scale such as upwelling events.

¹ An ADI – scheme is an Alternating Direction Implicit – scheme in which water properties are calculated implicitly and velocities are calculated explicitly. More details on the semi – implicit scheme can be found in chapter III.

II Review of literature

1. Introduction

This chapter focuses on the literature on the water masses of the Northeast – Atlantic off the Iberian Peninsula bounded by -12.67 & $- 5.53^{\circ}\text{W}$ and 34.3 & 45.03°N . The thermohaline structure of the study region presents three main layers; the upper, the intermediate and the deep layer. The upper layer is 100-200m thick and contains surface waters and ENACW (Eastern North Atlantic Water). Underneath these surface waters, the ENACW marks the thermo-halocline. Intermediate layers, below 500m of depth are dominated by Mediterranean Water (MW). Nevertheless, in the northwest of the Iberian basin, LSW (Labrador Sea Water), may be present at depths not exceeding 1600m. The deep layer is marked by various stages of mixing between MW, LSW and NADW overlying the homogenous deep layer of North Atlantic Deep Water (NADW). (Ambar & al., Theme 1)

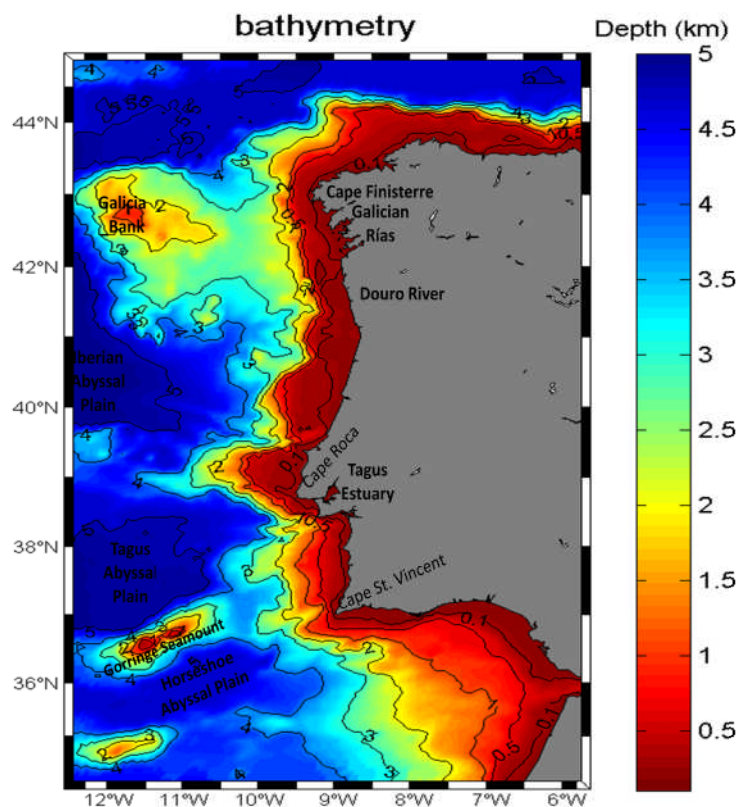


Figure 1: Bathymetry of the study region with the main topographic features

2. Water masses and their characteristics

2.1 Upper layer: Surface waters and central waters

The thickness of the upper layer varies widely from summer to winter as it is greatly influenced by run – off from land and convection. In winter, its depth from 700m in the north to 200m in the south due to the intensity of deep convection. Coastal upwelling on the other hand, occurs mainly in summer as a result of the northward migration of the Azores high.

In May 1993, the shallow thermocline is situated at about 20 – 30m in the north and at about 50 – 60m in the south. Below, remnants of the winter mixed layer can be found. This layer is homogenous and often marked by a salinity maximum at its deepest level. This subsurface salinity maximum can be traced throughout the study region between $\sigma_\theta = 26.95$ (see full arrows in figure 1 b, c, e and f). The isopycnal surface at $\sigma_\theta = 26.95$ was chosen to demarcate the surface layers. It lies at about 100-120m offshore in the centre and in the south of the study region at a depth of about 50 m. Another interesting feature is a secondary, shallower salinity maximum at $\sigma_\theta = 26.9$, between 50 and 90 m (see open arrows in figure 1 e & f). (Fíuza & al.,1998)

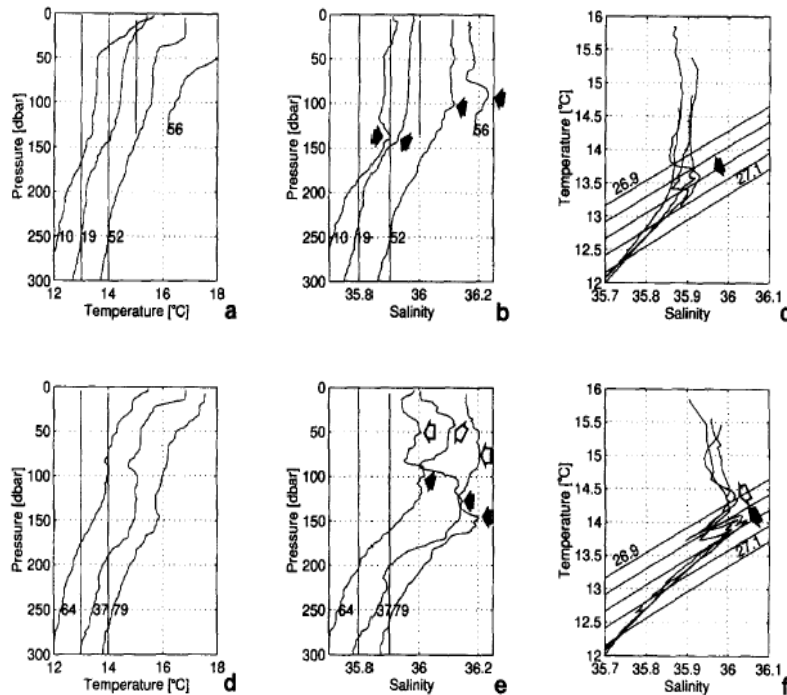


Figure 2: Examples of salinity and temperature profiles obtained in the north (45°N14°W, lower panel) and south (40°N,12°W, upper panel) surface waters (Fíuza & al., 1998).

The subsurface salinity maximum described above (at 50 – 80m) corresponds to the upper limit of the ENACW_{st}. The ENACW corresponds basically to the water of the permanent thermocline and consists of two water masses of different origins: a lighter, relatively warm and salty subtropical branch, the ENACW_{st}, and a less saline and colder branch known as ENACW_{sp}. The ENACW_{st} is formed at the Azores front along 35°N by strong evaporation and cooling in winter. It is subsequently advected into the region by the eastward Azores current and its poleward continuation and marked by $\theta = 13.13^\circ\text{C} - 18.50^\circ\text{C}$, $S = 35.80 - 36.75$ and $\sigma_\theta = 26.95 - 27.10$. The 27.10 isopycnal corresponds to a depth of about 250m and marks the lower limit of the ENACW_{st}. The subpolar branch of the central waters is related to the Subpolar Mode Water. It is formed in the eastern North Atlantic, north of 46°N, by winter cooling and deep convection. The transition point between both central water masses is defined at $S = 35.75$ and $\theta = 12.5^\circ\text{C}$. At more than 400 km from the western and northwestern Iberian shores, the ENACW_{st} is replaced by the fresher WNACW (Western North Atlantic Central Water).

2.2 Intermediate layer

The influence of the warm, salty Mediterranean water west off the Iberian Peninsula starts at 500 – 600m, where the salinity minimum corresponds to the lower edge of the Central Water. The Mediterranean water is divided into two main cores. The upper core is characterized by its temperature maximum of 13 °C and is centered at the $\sigma_\theta = 27.5$ isopycnal. The lower core on the other hand is marked by a salinity maximum of 36.2 and is centered at the $\sigma_\theta = 27.75$ isopycnal which correspond to a level of 1100 – 1300 dbar. The weakest signature of the two cores is found in the northwest of the MORENA - study region, whereas the southwestern part exhibits the strongest signatures. A shallow third core of Mediterranean water described by Ambar (1993) was not found in the CTD – data of the MORENA - campaign.

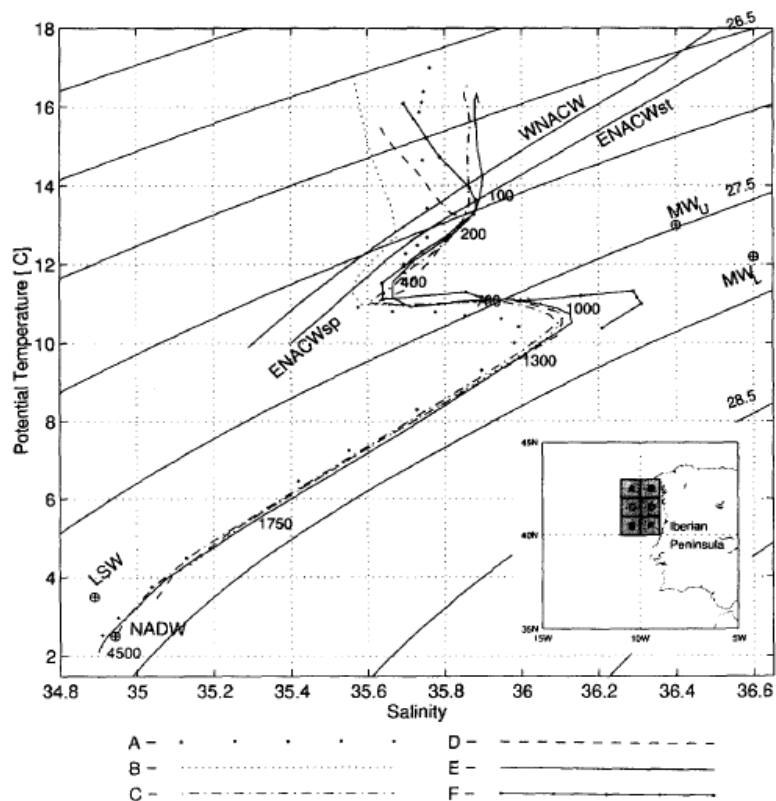


Figure 3: θ - S diagram of water masses off the Iberian Peninsula during May 1993 (Fiúza et al.,1998)

In the vicinity of the Galicia Bank, in the northwestern part of the region, Labrador Sea Water can be found. It is represented on the θ – S diagram by the kink towards lower salinities $S = 34.89$ and $\theta = 3.5^\circ\text{C}$.

2.3 Deep layer

As there are very few in situ data of deep water masses, literature on the deep layer is rather scarce. Various stages of mixing between MW, LSW and NADW are observed in this layer, thus leading to a slightly larger spreading of θ – S diagrams. The NADW has higher salinities and lower temperatures than the LSW and is defined by $\theta = 2.50^\circ\text{C}$ & $S = 34.943$.

3. Circulation

3.1 Upper layer: Surface waters and central waters

As northern winds start to dominate in spring, Coriolis force will deviate surface waters to the west, thus creating an upwelling along the west coast. This thin band of upwelled waters will force the slope current to leave the slope. The finger – like structures of upwelled water will gradually merge into larger filaments, 30 to 40 km wide and up to 250km long. These filaments are orientated offshore and may have different dynamic origins. Those anchored at the capes are due to topographical forcing, whereas in areas of smooth coastlines and bathymetry they are related to the evolution of frontal instabilities. The upwelling will also provoke a decrease of surface dynamic height towards the coast resulting in an equatorward geostrophic current. In the surface layer, this geostrophic current can counter the northward Portugal Slope Current (PC). However, underneath, waters between 100 – 200m waters still flow poleward. The south coast of Portugal is affected by a westerly wind which induces more intermittent upwelling events during late spring and summer. The intensity and frequency of upwelling events along the south coast decreases from west to east resulting in an eastward current during the upwelling season.

In autumn and winter the wind reverses resulting in a predominantly northward surface circulation. The weak northerly winds favor coastal convergence and hence downwelling. They are occasionally alternated with strong south-southwest winds. Although upwelling events are uncommon in winter, occasional upwelling events around Cape Vincent (37°N & 7°W) have been observed. (Ambar & al.,1993 , Peliz & al., 2002)

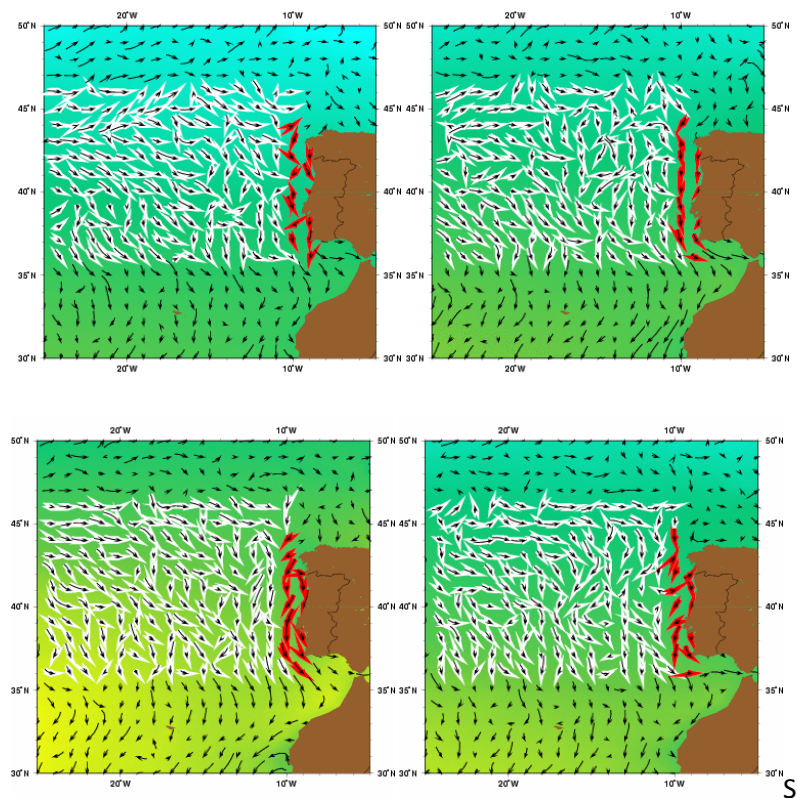


Figure 4: The Portugal current system in January-March, in May-June, in July-Sept and in Oct.-Dec
<http://oceancurrents.rsmas.miami.edu/atlantic/portugal.html>

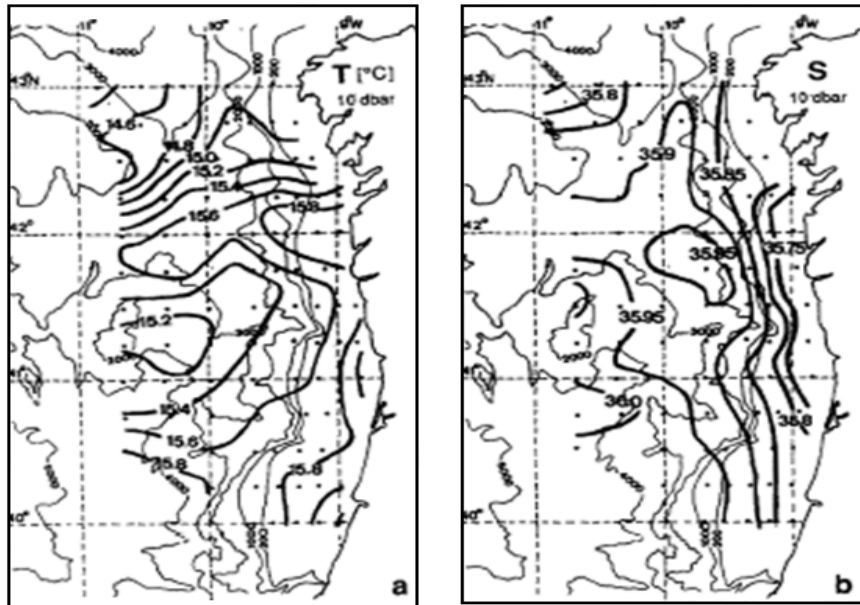


Figure 5: Distributions of temperature and salinity at 10dbar (Fiúza et al., 1998).

The near surface distributions of temperature and salinity at 10 dbar in May 1993 reveal a relatively warm saline tongue penetrating from offshore near 41°N. Part of this warm saline jet will turn to the south and follow the slope, although the majority will extend northward. This warm saline water (20°C and S=36) is separated from the low salinity water over the shelf by a density gradient. This frontal structure is strongly related to the topography and constrains the low salinity river run – off water to the shelf. On the shelf, weak northward flow related to fresher and cooler waters seems to dominate. These fresher and cooler waters are also known as the Western Iberian Plume (WIBP). The largest contributors to this plume are the Douro river and the Galician rias. In the south of the study region only the Tagus river represents a significant contribution to coastal shelf waters. Despite its name, the WIBP is in fact denser than offshore saline waters. Part of the WIBP is advected northward by the slope current and another part will leave the coast with the upwelling jet.

Central waters are characterized by a northward current which is partially driven by a meridional alongshore density gradient. This Portugal Coastal Countercurrent (PCC) carries relatively warm and salty subtropical waters along the continental slope at velocities around 0.2 – 0.3 m/s. It is marked by an increasing downstream transport and can be forced by a broad band of eastward geostrophic flow in the northeast Atlantic. The geopotential anomaly at 200 dbar reveals a geostrophic flow entering at 41 – 42°N that bifurcates on the slope before developing a southward branch and a poleward current. This poleward current, which is also known as the Portugal Coastal Countercurrent, represents a northward extension of ENACW_{st} and meanders along 10°W. It is very similar to the poleward flow in the vicinity of in winter season. In May 1993, the countercurrent was strongly perturbed by meanders and by an anticyclonic eddy at 40.75°N. In the northwest of the study region, north of 42.7°N and west of 10°W, a major oceanic front was present at central water levels. This Galicia front is the northern boundary form ENACW_{st} and constitutes a downward extension of the front in surface layers. North of the Galicia front, ENACW_{st} is replaced by WNACW. Between 300 & 600m of depth, the east – west orientated front bends north to the shelf edge, which suggests a narrow vein of northward moving water near the shelf edge.(Fiúza & al.,1998)

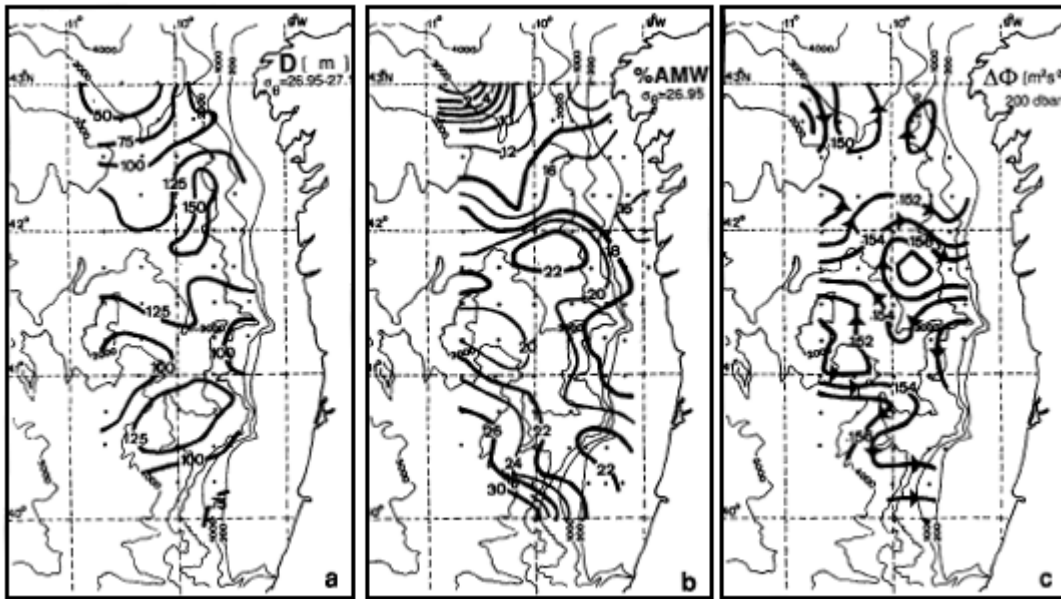


Figure 6: Thickness of the layer of ENACW_{st} , % of Azores Mode Water in the ENACW_{st}, the geopotential anomaly at 200 dbar relative to 350 dbar (Fiúza et al., 1998).

3.2 Intermediate layer

As the Mediterranean water leaves the Strait of Gibraltar and descends along the slope it is subjected to turbulent mixing. The dramatic bathymetry quickly divides the Mediterranean outflow into three veins, a shallow vein at about 400m, an upper core of at 700m and a lower core at 1200m. The shallow core quickly dissipates as it does not represent a significant volume and experiences a lot of interaction with surrounding water masses. The characteristics of this core have never been observed north of the Tagus estuary. The characteristic maxima of temperature and salinity associated with the upper and lower core of Mediterranean water are also progressively depleted along their northward path along the Iberian Peninsula. The temperature maximum of the upper core decreased from 11.5 to 10.9°C at 0.24°C/km while the salinity maximum of the lower core varied from 36.2 to less than 36 at 0.06/100km. The depth of the salinity maximum of the lower core subsequently decreased from 1200m in the south of the study region to 1000m in the north, whereas temperature decreased from 11 to 10°C at 0.05°C/100km. A possible explanation for this temperature gradient being lower than that of the upper core is that the dominant mixing process in the upper core is temperature diffusion, whereas in the lower core, double diffusive mixing of salinity prevails. (Bower & al., 2002)

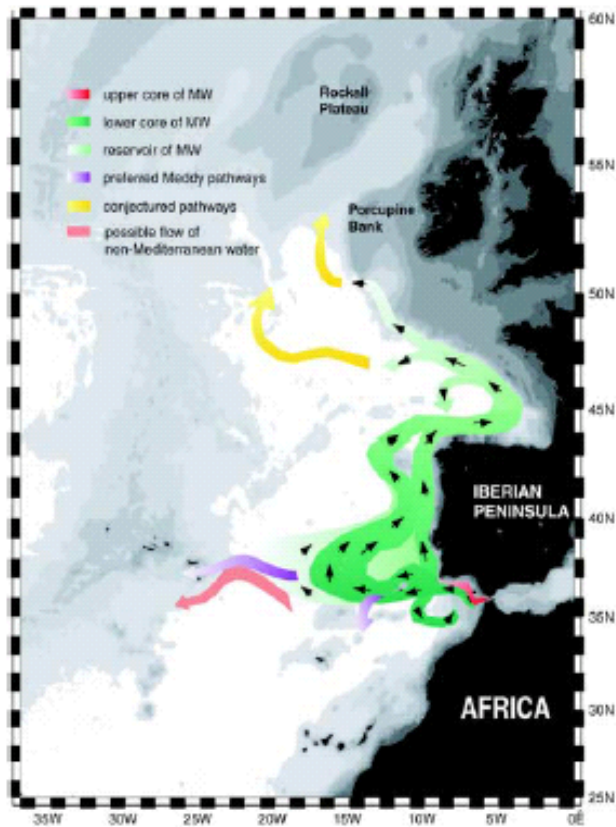


Figure 7: Pathways of Mediterranean water as observed by AMUSE (Bower & al., 2002)

The Mediterranean outflow in the Gulf of Cadiz is mostly constrained to the Iberian slope by the horizontal component of the Coriolis force. Once the two remaining cores have rounded Cape St. Vincent, their temporary hydrostatic equilibrium will no longer be perturbed and they continue their northward path as geostrophic flows. Between 40 & 43°N, the Mediterranean waters seem to be confined to the slope by the intrusion of low salinity Atlantic waters. As a consequence, only a narrow vein of Mediterranean water will round Cape Finisterre.

3.3 Deep layer

The deep layer mainly consists of NADW and lesser quantities of LSW. The percentage distributions of both water masses and the thermohaline characteristics of the deep layer are given by figure 8. At this level, the signature of the Mediterranean Water was still detectable on the slope as far north as 42.5°N, although it was strongly weakened. In the vicinity of the Galicia Bank we can notice the influence of the Labrador Sea Water. The LSW subsequently moves south to the region, thus forming a lateral salinity gradient between 42-43°N with the NADW. This lateral salinity gradient is still highly influenced by the overlying MW. At about 42°N, the zonal salinity gradient between both deep water masses weakened as a consequence of the westward penetration of the more saline NADW. As this observation is coherent with the tendencies of the lower core of MW, this confirms the downward extension of its influence. The lower core of MW even constitutes 10 – 15% of the total volume at 1800m of depth, while the majority (85 – 90%), can be attributed to the genuine deep layer water masses (the NADW and the LSW). (Peliz & al., 2002, Hutchance & al., 2002)

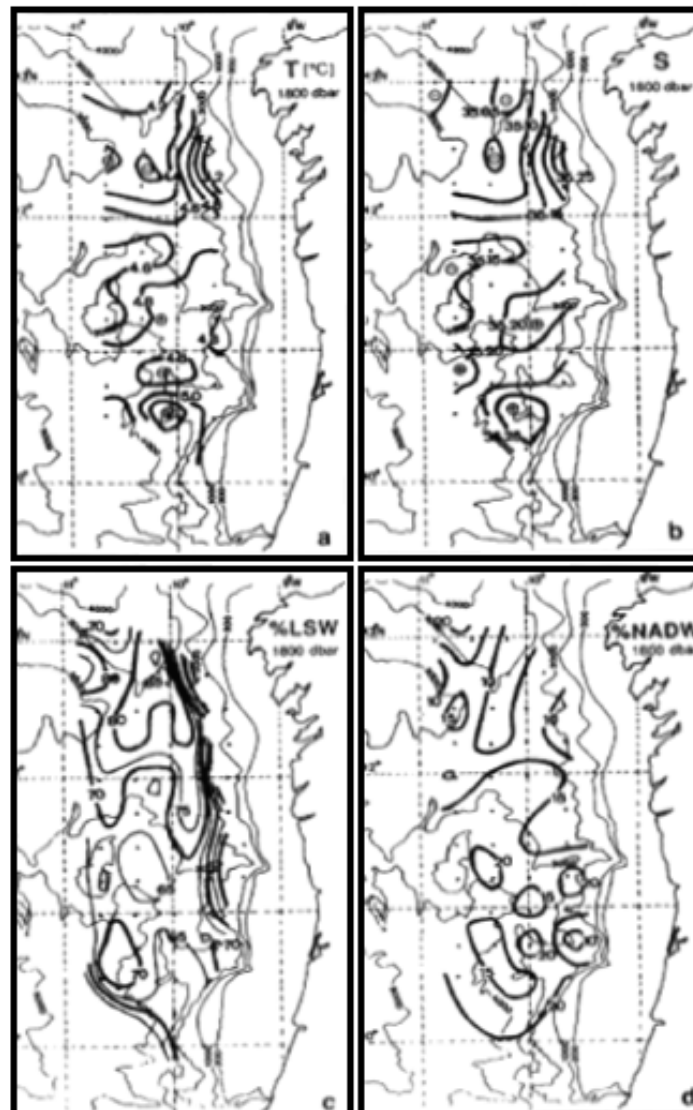


Figure 8: Percentage distributions of the different water masses and thermohaline characteristics of the deep layer at 1800 dbar (Fiúza & al., 1998)

4. Quantification

Although upper water masses in the study region have been described elaborately, there are only very few studies describing transports. As transports often include several water masses, the only water mass to have been accurately quantified is the Mediterranean Outflow through the Strait of Gibraltar. Bryden (1994) estimated this outflow at 0.7 Sv. The subsequent poleward transport of Mediterranean waters over the Portuguese shelf between 39 – 41°N has been quantified by Stevens (2000) at 1.2 Sv. Although this seems contradictory, these differences in transport can be explained by the fact that Bryden calculated the mass budget for waters with a salinity of at least 36.1, while Stevens included all volumes having a salinity greater than 35.95. Due to the steep topography of the Iberian Peninsula, Mediterranean waters experience a lot of mixing with surrounding waters. As a consequence Stevens' model also included the waters entrained by the MW. Stevens also made estimations of the poleward transport in the surface layer (which he defines as 0 – 333m of depth). At 39°N he found a transport of 0.14 Sv which intensifies to 0.28 Sv at 41°N and 0.37 Sv at Cape Finisterre (43°N). Data on vertical transports is even scarcer as these transports represent even smaller volumes. The only estimates of Ekman upwelling off the Portuguese coast are given by Mazé (1997). He estimates the summer upwelling at 0.2 Sv. A schematic overview of these vertical transports is given by figure 9.

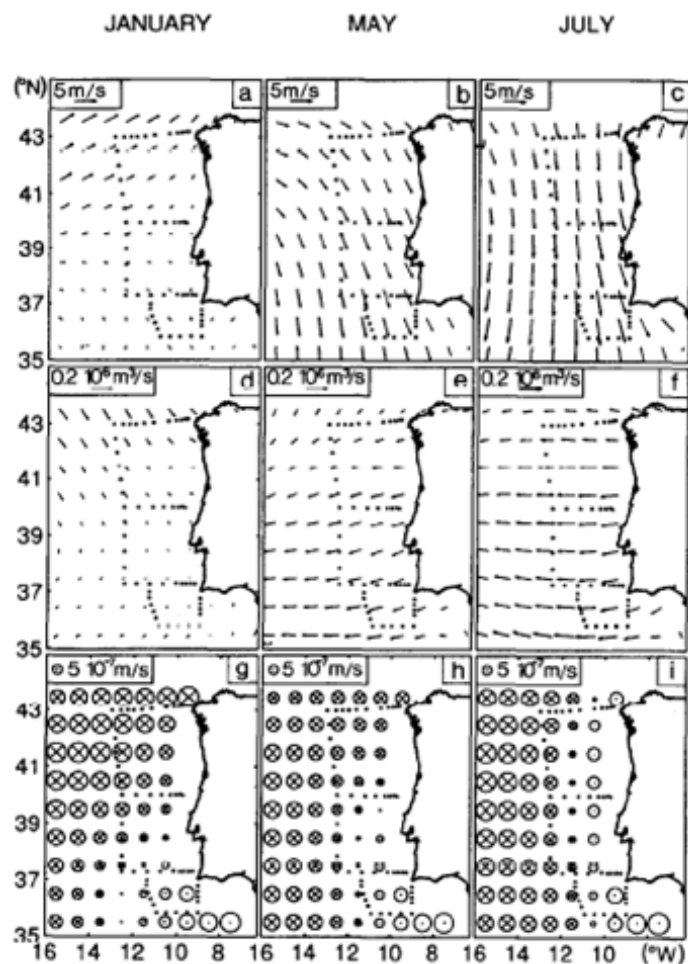


Figure 9: Wind, Ekman transport and Ekman transport per degree of latitude calculated by Mazé & al., 1997.

5. Discussion

The hydrologic structure of the waters off the Western Iberian Peninsula is characterized by three main layers, the upper, the intermediate and the deep layer. The upper layer is divided into surface waters (0-100m), ENACW_{st} (100-250m) and ENACW_{sp} (250 – 650m). Below 500m we also start to notice the influence of the Mediterranean waters. These Mediterranean waters are the main water mass of the intermediate layer (650 – 1600m). The upper core of Mediterranean water is characterized by a temperature maximum and can be found at about 800m of the depth. The lower core is situated at about 1200m of depth and has a distinct salinity maximum. In the vicinity of the Galicia bank, at depths not exceeding 1600m, there is also a contribution of LSW to the intermediate waters. The deep layer (>1600m) consists of an upper deep layer (1600 – 1900m) marked by various stages of mixing between MW, LSW and NADW overlying the homogenous lower deep layer of NADW. Finally, in order to make a distinction between abyssal plains and zones with a more important topography, we shall also make a distinction between waters above and below 3000m. We also should remark that these depths are no absolute boundaries between different water masses, they are mainly indications of interface depths. In the next chapter, we shall use these indicator depths in the parameterization of the MOHID – model.

III Data and methods

1. Introduction

In this chapter we will discuss the methods applied to input and output data and the characteristics of the MOHID - model. The model consists of a pre – processing module which provides all necessary data to run the model, a processing module that calculates all output data we will use to analyze in the post – processing module. The pre – processing module provides the barotropic model with ETOPO 2 bathymetry and FES 2004 tidal data. This 2D model will supply the 3D baroclinic model with sea surface height, barotropic velocities to apply boundary conditions. This baroclinic model will also require temperature and salinity fields from the Mercator model, river data and atmospheric forcing in order to calculate output data. The output data consists of hdf5 – files of hydrodynamic and water properties and of text – files of fluxes through pre – defined boxes. These boxes are defined in function of the different water masses of the Western Iberian Peninsula and are further discussed in section 2 of this chapter.

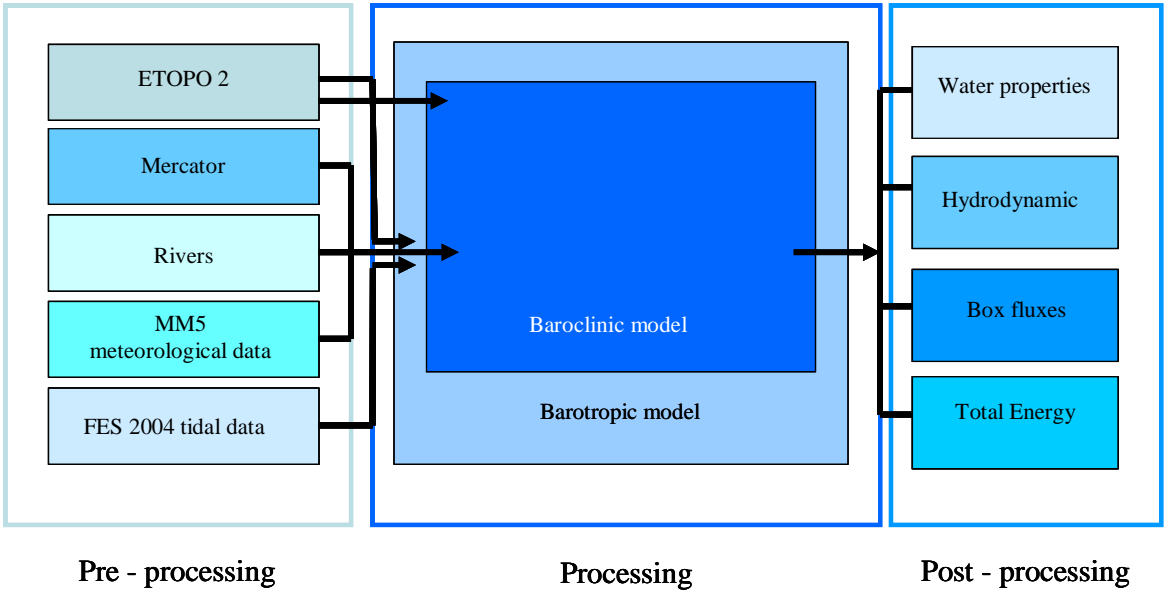


Figure 10: Schematic overview of the MOHID - model

2. Spatial discretisation

The domain of the MOHID - model is bounded by -12.67 & -5.53°W and 34.3 & 45.03°N . The original horizontal and vertical grids of the model were adapted in order to better identify the different water masses described in chapter II. Vertical layers were chosen to vary exponentially from indicator depths. These indicator depths also mark the boundaries of the 7 vertical boxes used in this simulation. Horizontally the different water masses are mainly influenced by topography. Therefore we used the MOHID – GIS program to demark 22 horizontal boxes in the horizontal grid which consists of 117×177 grid cells. Then we had to link vertical to horizontal boxes. This is done manually by reading the maximum depth of each horizontal box in MOHID – GIS and by associating the necessary number of vertical boxes in a data-file which will be introduced into MOHID.

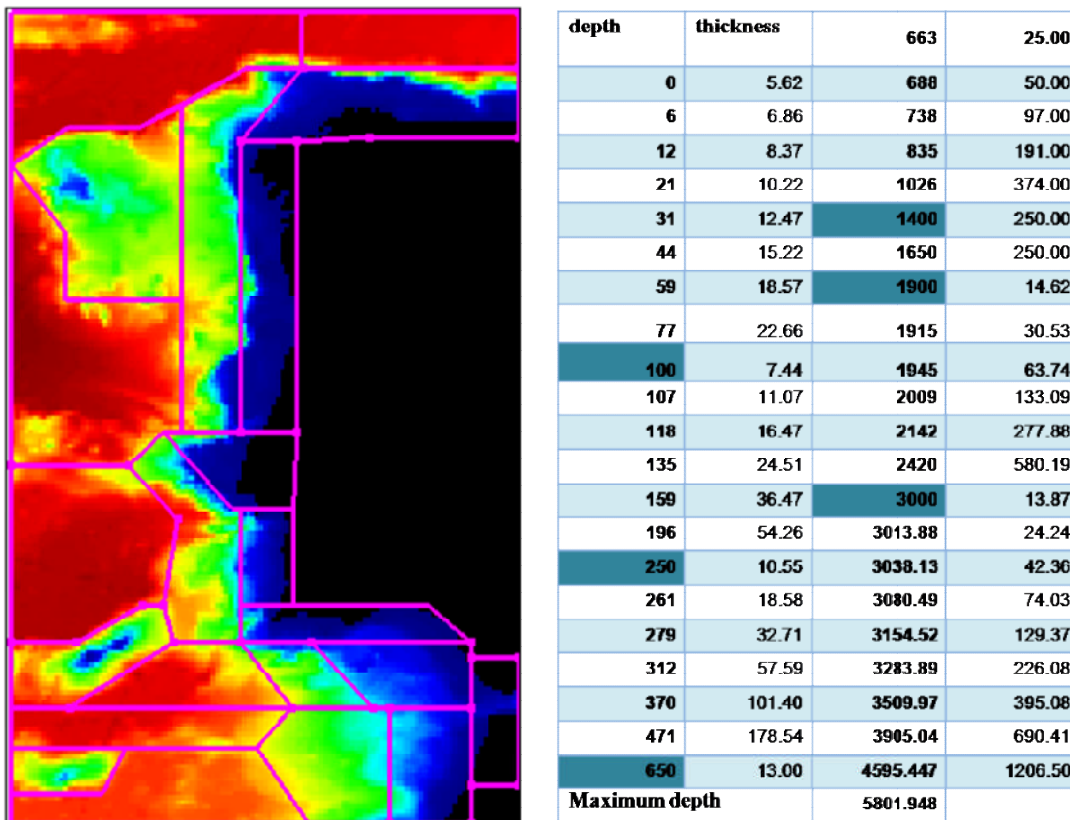


Figure 11: Horizontal and vertical boxes used in this MOHID simulation

3. Pre – processing

3.1 ETOPO 2

The bathymetry used by MOHID is the ETOPO 2 – bathymetry with a resolution of $2'$.

(N.Etopo Bathymetry 1988)

3.2 Mercator

Mercator provides the MOHID – model with continuous fields of salinity, temperature, velocity u , velocity v and water level for the entire domain. These data will be interpolated to fit the newly developed vertical grid. Barotropic velocities acquired for the Flather radiation condition, will be generated from this interpolated file with the HydrodynamicAnalyser - tool.

Mercator uses Smith & Sandwell '97 bathymetry with a resolution of 1 minute. The model consists of 43 vertical levels with layer thickness ranging from 6m at the surface to 300m at the bottom. The horizontal resolution is 5 to 7 km. Atmospheric forcing is provided by the operational analysis of ECMWF – data which provides daily data of wind stress, solar radiation, total heat flux (solar insolation, IR, sensible & latent heat flux), evaporation and precipitation. As the PSY2V2 – version of Mercator we used to force MOHID applies a rigid lid condition at the sea surface, it does not include any tidal functions. Initial conditions are provided by Reynaud climatology, which provides monthly temperature and salinity fields at 1° resolution. In the Strait of Gibraltar the cartesian coordinate model applies a small relaxation to climatological values in order to better approximate the characteristics of sinking Mediterranean waters (Drillet & al., 2005).

3.3 Rivers

In order to obtain a realistic approach to the different water masses of the Iberian Peninsula, rivers with significant fates have to be included. Thus, the Tagus river, the Douro river and Galician rivers are introduced into the model. Daily mean fates and mean air temperature were obtained from SNIRH. Then, data gaps in river fates were overcome by linear interpolation in the case of small gaps and in case of a data gap of two or more subsequent days, the following function was applied:

$$C_A = \beta_0 + \beta_1 S_1 + \beta_2 S_2 + \varepsilon$$

Beta coefficients were obtained by introducing this algorithm into a statistical program (R 2.6.2) and S_1 & S_2 are fate values of neighbouring stations and ε is the unknown error of approximation. Then, we approached these continues series of river fates and atmospheric temperature by polynomials of the fifth degree. This approximation allows us to extract the seasonal cycle and to eliminate daily and weekly variations. For simplicity, polynomials of river fate and air temperature were introduced into a single cell in the middle of the river delta at a depth of 59m.

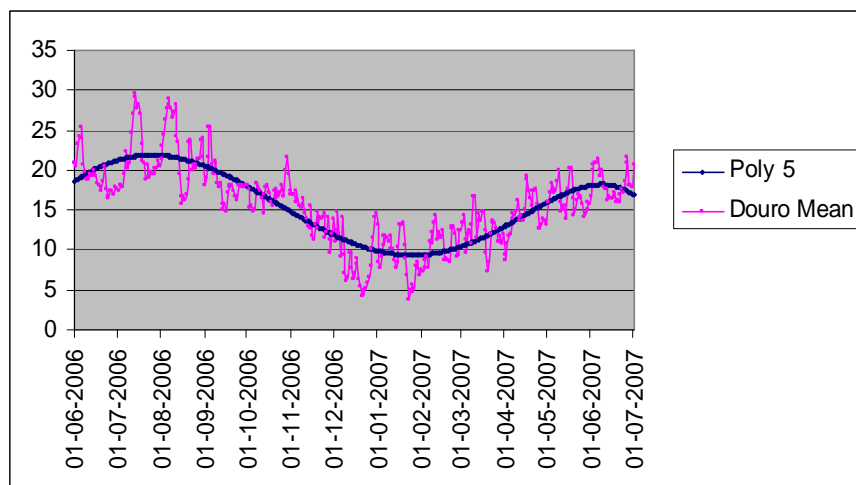


Figure 12: Mean daily Douro temperature and a polynomial of the fifth degree

3.4 Numerical weather forecast model “MM5”

The MM5 - model is a three-level nested mesoscale atmospheric model for the domain bounded by 28°N & 50°N and 20°W & 5°W. The pre-processing module of the model consists of five sub-modules. The TERRAIN - module defines terrestrial domains, soil type (which defines the albedo) and topography, and interpolates them horizontally onto a regular grid. The REGRID - module interpolates meteorological data at different pressure levels or at the surface of the different domains horizontally. The meteorological data being used are either AVN (Global Aviation Model) or NCEP (USA National Centres for Environmental Protection), although more recently, the AVN data was replaced by GFS - data (Global Forecast System) and the model was also forced by ECMWF - data (European Center for Medium - Range Weather Forecasts). LITTLE - R is a module which allows us to enhance the initial data with observations of mean sea level pressure, wind direction and velocity temperature and dew point. In order to verify the quality of observational data, it is being compared to the nearest points in the meteorological data grid before being added to the data set. Initial and boundary conditions are provided by the INTERPF - module. This program calculates various surfaces sigma, S, in function of altitude, z, and interpolates data of adjacent isobaric surfaces vertically onto constant sigma surfaces. It also calculates additional variables required by the non - hydrostatic model such as the vertical wind velocity and perturbations of atmospheric pressure.

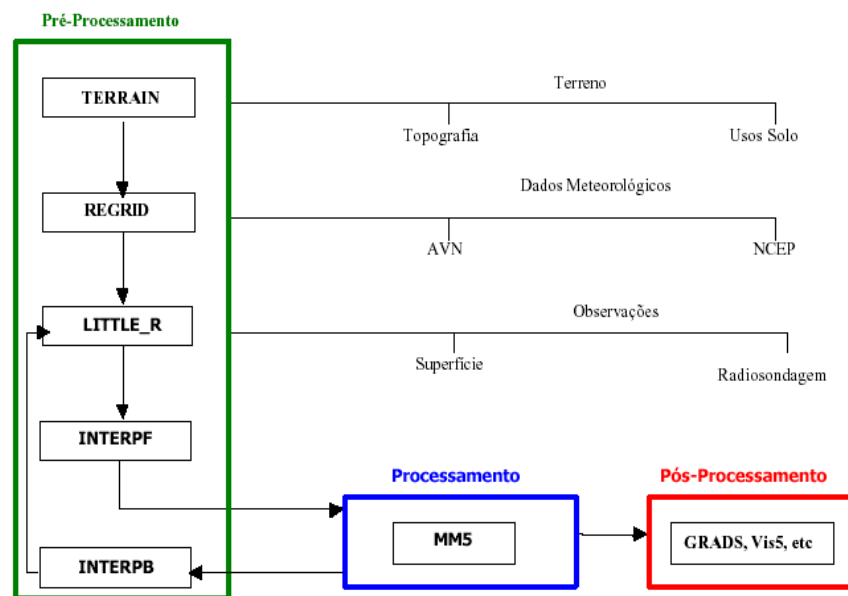


Figure 13: Schematic overview of the MM5- weather forecast model

The MM5 - processing module is the program that develops numerical predictions by resolving the three-dimensional Navier - Stokes equations, the thermo-dynamical equation and the conservation of water mass in the sigma coordinate system. Parameterisation of physical processes, clouds, precipitation, boundary layer and radiation is also being defined in this program. This module provides MOHID with continuous fields of wind velocity, sensible heat, latent heat, solar radiation, precipitation, evaporation, specific humidity, cloud cover and atmospheric pressure at a resolution of 81km (D1), 27 km (D2) and 9 km (D1). In order to refine the resolution, the smaller domains are integrated into the larger domains by means of the ConvertToHdf5 - tool. (Sousa, 2002; Riflet & al., 2007)

3.5 FES 2004

FES2004 provides MOHID with tidal predictions for the main tidal constituents at a resolution of $1/8^\circ$. It consists of the CEFMO (Code aux Eléments Finis pour la Marée Océanique) & CADOR (Code d'Assimilation de Données orientées Représenteur) – models and altimetry data. The boundary conditions for the water levels of CEFMO and CADOR models are given by the NSWG – model or by the geodetic satellite empirical model (GEOSAT). In dynamically complex regions tide gauge data is being implemented. The models offer basin – scale solutions for semi – diurnal M_2, S_2, N_2, K_2 & $2N_2$ constituents (CEFMO) and for diurnal K_1, O_1, Q_1 and P_1 constituents (CADOR). (Lyard & al., 2006)

In the study region M_2 and S_2 are the dominant constituents, although in some parts over the continental shelf diurnal harmonics and especially K_1 can become important. The K_1 constituent can alter M_2 and S_2 tidal current patterns significantly and is most considerate over the Lisbon promontory. (Marta – Almeida & al., 2006)

4. MOHID

4.1 Equations

The MOHID – model solves the Navier Stokes equations of a rotating fluid in a β – plane. Navier Stoke equations and equation for conservation of mass are given by:

$$\rho \frac{Du}{Dt} + \rho \Omega \wedge u = -\nabla p - g \rho e_z - \nabla \cdot F^v$$

$$\frac{\partial \rho}{\partial t} + \nabla \cdot (\rho u) = 0$$

With ρ , the density, u , the velocity, Ω , the earth's rotation, g , the acceleration of gravity and F^v turbulent viscous forces. By applying Boussinesq approximation, we obtain the non - hydrostatic equations of conservation of mass and conservation of momentum:

$$\nabla \cdot u = 0$$

$$\frac{du}{dt} + \Omega \wedge u = -\frac{1}{\rho_0} \nabla_h p - \frac{gp}{\rho_0} e_z - \frac{1}{\rho_0} \nabla \cdot F^v$$

Where ρ_0 is the reference density and ∇_h is defined as

$$\nabla_h = e_x \frac{\partial}{\partial x} + e_y \frac{\partial}{\partial y}$$

The velocity u can be decomposed in a horizontal and a vertical component:

$$u = v + w e_z$$

By using a decomposition of Reynolds, we acquire

$$\frac{du}{dt} - fv = -\frac{1}{\rho_0} \frac{\partial p}{\partial x} + \nu_h \left(\frac{\partial^2 u}{\partial x^2} + \frac{\partial^2 u}{\partial y^2} \right) + \frac{\partial}{\partial z} \left(\nu_v \frac{\partial u}{\partial z} \right)$$

$$\frac{dv}{dt} + fu = -\frac{1}{\rho_0} \frac{\partial p}{\partial y} + \nu_h \left(\frac{\partial^2 v}{\partial x^2} + \frac{\partial^2 v}{\partial y^2} \right) + \frac{\partial}{\partial z} \left(\nu_v \frac{\partial v}{\partial z} \right)$$

$$\frac{dw}{dt} = -\frac{1}{\rho_0} \frac{\partial p}{\partial z} - \frac{g\rho}{\rho_0} + \nu_h \left(\frac{\partial^2 w}{\partial x^2} + \frac{\partial^2 w}{\partial y^2} \right) + \frac{\partial}{\partial z} \left(\nu_v \frac{\partial w}{\partial z} \right)$$

Herein is ν the turbulent viscosity. The horizontal turbulent viscosity is constant, whereas the turbulent vertical viscosity is computed by the model. Finally, we apply the hydrostatical approximation to the vertical velocity in order to obtain primitive equations:

$$\frac{\partial p}{\partial z} = -\rho g$$

The Coriolis parameter in the non – hydrostatic equations is given by:

$$f = 2\Omega \sin \lambda$$

As f is a function of the latitude λ , we can write its variation around a central latitude:

$$f = f_0 + \beta y$$

Where β is defined as:

$$\beta = \frac{2\Omega \cos \lambda_0}{R}$$

(Barth, 2008) (Kundu, 3rd edition)

4.2 Initial conditions

Initial conditions for salinity and temperature are derived from the PSY2V2-version of the Mercator-model. Initial values of water level and velocities are zero. During spin-up time, the model is forced by the wind stress, solar radiation, and by the external data, namely water level, velocities u & v and temperature & salinity. Thus, in order to smooth out the numerical noise introduced by the unbalanced horizontal pressure gradient in the initial field, the pressure gradient force and the wind stress are activated very slowly, after 43200 seconds. Given the realistic continuous density, velocity and water level fields, the spin-up period is rather short energetically speaking. The kinetic energy stabilizes at 8.10^{15} Joules after about 6000 output time steps. As the model provides us with values of kinetic energy every 10 minutes, spin – up time equals 41.67 days. (Leitão et al 2006)

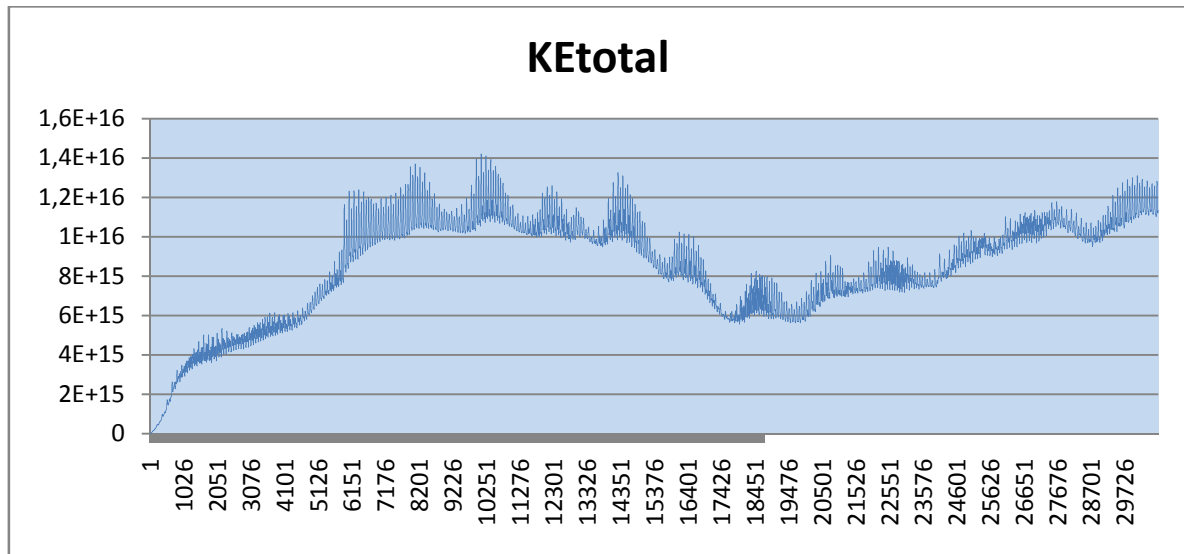


Figure 14: Total kinetic energy of the simulation

4.3 Boundary conditions

As MOHID comprises both a barotropic and a baroclinic model, different boundary conditions will be applied. For the 2D barotropic model we use the radiation method of Blumberg & Kantha (1985). For the water level, the boundary condition is given by

$$\frac{\partial \eta}{\partial t} + \left(\vec{c}_E \cdot \vec{n} \right) \nabla \eta = \frac{1}{T_d} (\eta^{\text{ext}} - \eta)$$

With $c_E = \sqrt{gh}$, the celerity of the surface wave, η the water level and T_d the time of decay. For a flow entering the domain, we should also force the water level with the tidal information obtained from FES 2004.

The 3D barotropic model is bounded by the Flather radiation method for water levels and barotropic flow.

$$q - q^{\text{ext}} = (\eta - \eta^{\text{ext}}) \left(\vec{c}_E \cdot \vec{n} \right)$$

Where q is the barotropic flow, η the water level and $c_E = \sqrt{gh}$ is the celerity of the surface wave.

Barotropic velocities are restrained by

$$v_{\text{barotropic}} = q_{\text{barotropic}} / H_f$$

Herein is $q_{\text{barotropic}}$ the barotropic flow and H_f the total height of the water level (level at rest + elevation). External reference values for water level and velocities are provided by the barotropic model and by the PSY2V2 – Mercator model. We also enforce a flow relaxation scheme for salinity, temperature and total velocities (u & v).

$$\frac{\partial \vec{v}}{\partial t} = \sum \text{Forces} + \frac{\vec{v} - \vec{v}^{\text{ext}}}{T_d}$$

With v the total horizontal velocity and T_d the time of decay. For water properties the equation becomes:

$$p^{t+\Delta t} = p^* + (p^{\text{ext}} - p^*) \frac{\Delta t}{T_d}$$

With P the water property and T_d the time of decay. The relaxation zone covers 10 grid cells and is given by figure 15.

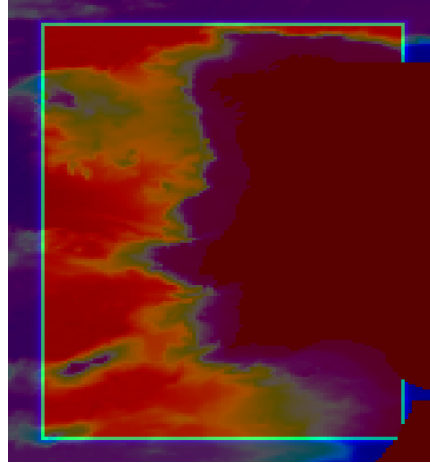


Figure 15: Relaxation zone of the MOHID - model

As we do not use any relaxation for baroclinic internal gravity waves, we apply a sponge layer to the outer ten grid cells in order to attenuate reflected spurious baroclinic flow oscillations. (Marchesiello, 2001, Leitão 2003, Riflet, 2007)

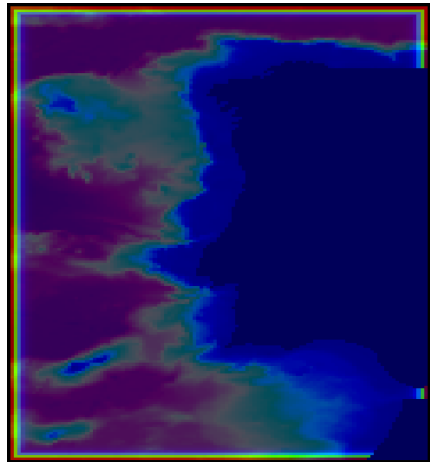


Figure 16: Sponge layer of the MOHID - model

4.4 Numerical schemes

MOHID utilises an Arakawa C grid. Water level & water properties are thus calculated in the centre of the grid cells, whereas velocities are calculated at in between grid cells. The model applies a semi – implicit ADI scheme to discretise in time and a TVD – scheme to discretise in space.

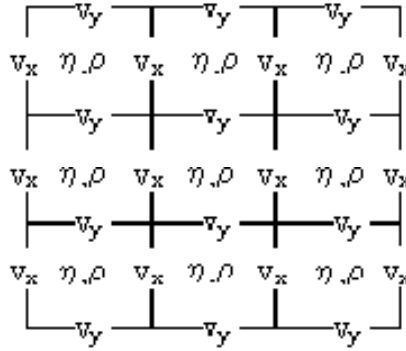


Figure 17: The Arakawa C grid

The semi – implicit ADI scheme is an iterative scheme MOHID uses to calculate the water level and vertical and horizontal velocities. A common Alternating Direction Implicit – scheme adds an extra term containing the first time derivative to the equation ($t+\Delta t$). The semi – implicit scheme will add terms calculated in ($t+\Delta t/2$), thus rendering the scheme more stable. The basic semi – implicit scheme consists of the following equations:

1st pass:

$$\begin{aligned} & (-A^i P_{i+1,j})^{t+\Delta t/2} + ((1 + B^i) P_{i,j})^{t+\Delta t/2} + (-C^i P_{i-1,j})^{t+\Delta t/2} \\ & = (A^i P_{i,j+1})^t + ((1 - B^i) P_{i,j})^t + (C^i P_{i,j+1})^t \end{aligned}$$

2nd pass

$$\begin{aligned} & (-A^i P_{i,j+1})^{t+\Delta t} + ((1 + B^i) P_{i,j})^{t+\Delta t} + (-C^i P_{i-1,j})^{t+\Delta t} \\ & = (A^i P_{i+1,j})^{t+\Delta t/2} - ((1 - B^i) P_{i,j})^{t+\Delta t/2} + (C^i P_{i-1,j})^{t+\Delta t/2} \end{aligned}$$

This scheme is carried out in different legs. The semi – implicit expression will first calculate $u_1^{t+1/2}$, which is then used to compute the water level. Secondly, we deduct $u_1^{t+1/2}$ in order to calculate the vertical velocity $u_3^{*t+1/2}$. Finally, this vertical velocity is adapted to the modified water level. The resulting vertical velocity is thereafter being used to compute temperature and salinity fields in $t + 1/2$.

The implicit equation will derive from the semi – implicit equation and use it to calculate the implicit water level. The latter will be used to compute , which will allow us to find a solution for the vertical velocity . Finally, after adaptation for the modified water level, we obtain implicit temperature and salinity fields. (Leitão, 2002)

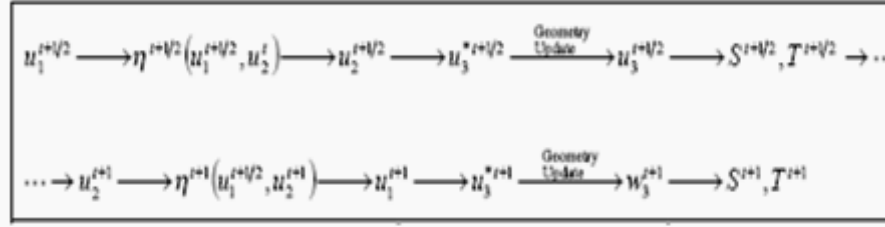


Figure 1: Leendertse discretisation of a semi - implicit ADI scheme

Spatial discretisation for advection is carried out by means of a TVD – superbee scheme. The program is said to be Total Variation Diminishing if:

$$TV^{n+1} \leq TV^n$$

$$TV^n \equiv \sum_i |C_{i+1}^n - C_i^n|$$

The first order upwind equation is thus TVD if $0 \leq a_{i+1/2}$, $0 \leq b_{i+1/2}$ and $a_{i+1/2} + b_{i+1/2} \leq 1$

$$C_i^{n+1} = C_i^n - a_{i-1/2}(C_i^n - C_{i-1}^n) + b_{i+1/2}(C_{i+1}^n - C_i^n)$$

For the TVD - scheme of superior order, the equation becomes:

$$\hat{C}_{i+1/2}^H = C_i^n + \Phi_{i+1/2} (\hat{C}_{i+1/2}^H - C_i^n)$$

Herein is $\hat{C}_{i+1/2}^H$ computed by a scheme of superior order and $\Phi_{i+1/2}$ is limited by:

$$\Phi_{i+1/2} = \max(0, \min(1, 2r_{i+1/2}), \min(2, r_{i+1/2}))$$

$$r = \frac{C_i - C_{i-1}}{C_{i+1} - C_i}$$

With

In the case of $\Phi = 0$, the model will use a first order upwind scheme and if $\Phi = 1$, we will apply a third order upwind scheme given by:

$$\hat{C}_{i+1/2}^H = \frac{-C_{i+2} + 9C_{i+1} + 9C_i - C_{i-1}}{16}$$

This scheme has the advantage that it tempers local extrema, thus minimising the overshooting of the dynamic equilibrium of the system and producing more realistic tracer patterns. (Holland & al.,1998, Beckers, 2007)

In order to complete the equations of spatial discretisation, we should add a diffusion term to the upwind schemes. Diffusion is given by:

$$J = -K \cdot \nabla C + \nabla_h (\kappa_4 \nabla_h^2 C)$$

Where the first term is the three – dimensional Laplacian diffusion and the second term represents the biharmonic mixing by the numerical scheme. As the biharmonic term is used to limit the number of spurious maxima and minima in the numerical solution, it is only two dimensional. The disadvantage of this biharmonic term is that it lacks positiveness and monotonicity which will lead to unphysical behaviour of the solution. (Delhez & al., 2007)

The MOHID – model will use a fixed horizontal diffusion, while vertical diffusion is calculated with the GOTM – module (General Ocean Turbulence Model). This module will gradually adapt the turbulent viscosity in order to ensure turbulent closure of the model.

5. Output of the MOHID – model

After resolving the previous equations, the MOHID – model provides us with two hdf5 – files, one for the hydrodynamic and one for the water properties, which give us 12 – hourly values of temperature, salinity, velocities, residual velocities and water level on our pre – defined spatial grid. Volume fluxes through pre – defined boxes are supplied by a simple text file which contains both instantaneous and monthly residual fluxes. As continuation of calculus is guaranteed by the simulation, its initial fields of salinity, temperature and barotropic velocities in June 2006 are supplied by Mercator. Afterwards, the model will use the solution of the preceding month to force initial conditions.

We also ensured the model is conserving mass by checking if the total volume of all boxes remains constant (see electronic appendix). As this is the case, mass is conserved.

III Validation of results

1. Introduction

The validation of results is indispensable to any simulation. A thorough validation of obtained results does not only give us an idea of the accuracy of the MOHID – model, it also helps explain why certain biases between model results and validation data exist. As data of transports along the Portuguese coast are virtually inexistent, we shall validate for temperature, salinity and velocities. Due to the lack of in situ data of the Iberian shelf, we shall first compare model results to annual climatology and to the Mercator - model. Although these comparisons are also subject to the errors of climatology and the Mercator – model, they give a good estimate of the reliability of MOHID – results in the entire domain. Afterwards we shall compare the results to the scarce in – situ date of the MORENA – campaign and to the data provided by Argo – floats.

2. Validation with climatology

In order to compare the model’s data to the annual climatology used in Juliano (2007), we first need to interpolate the climatological data to the grid used in the simulation. Subsequently, we had to average two daily temperature and salinity fields and monthly residual velocities. Eventually, we obtained the bias by subtracting MOHID - data from annual climatology. At the surface and in the surface layers, significant differences in salinity and temperature are mainly present in the relaxation zone of the Mercator – model. In this region, Mercator applies a relaxation to the Reynaud – climatology. MOHID uses these Mercator - solutions in order to initialize its temperature and salinity fields. The bias in velocity is mainly constrained to the Gulf of Cadiz and the Gorringer seamount where the geostrophic speeds provided by the climatology do not take into account the topographical forcing to which residual velocities are subjected.

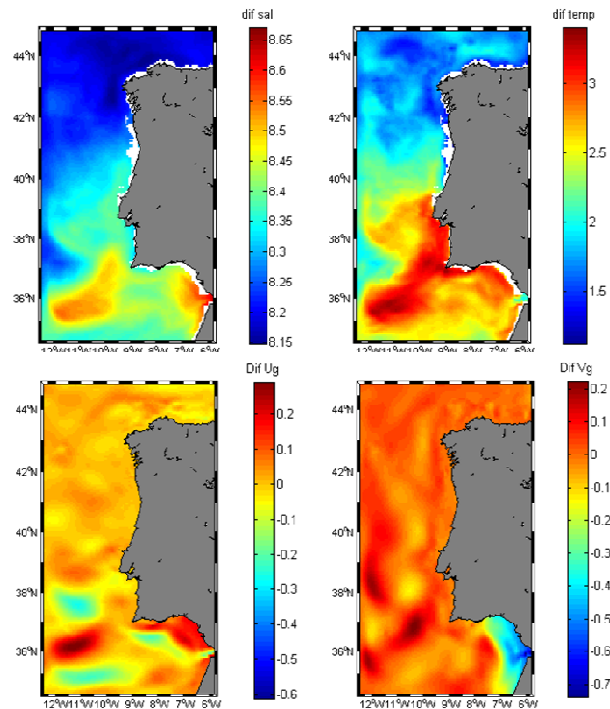


Figure 19: Comparison between annual climatology and the MOHID – model for fields of salinity (upper left panel), temperature (upper right panel) and velocity fields U (lower left panel) and V (lower right panel) at 8m of depth.

At 650m of depth, temperature and salinity biases are still more pronounced in the relaxation zone. The difference in velocity around Gorringer seamount is now more pronounced, as the intense residual currents in this zone will generate spurious positive and negative currents before and behind the seamount, thus creating a large negative and positive bias. The error in meridional velocity at 38°N might be due to the boundary conditions imposed to the MOHID – model for the barotropic flow. If the relaxation to barotropic velocities at the frontier is too strong, this will generate large differences between MOHID and Mercator values. Finally, we also notice very local differences along the shelf edge due to different bathymetries. These property tendencies were also present at 1400m of depth, after which they decreased slowly with depth (0.5°C/100m and $\Delta S = -0.18/100m$), whereas differences in velocity increased due to the rising importance of topography.

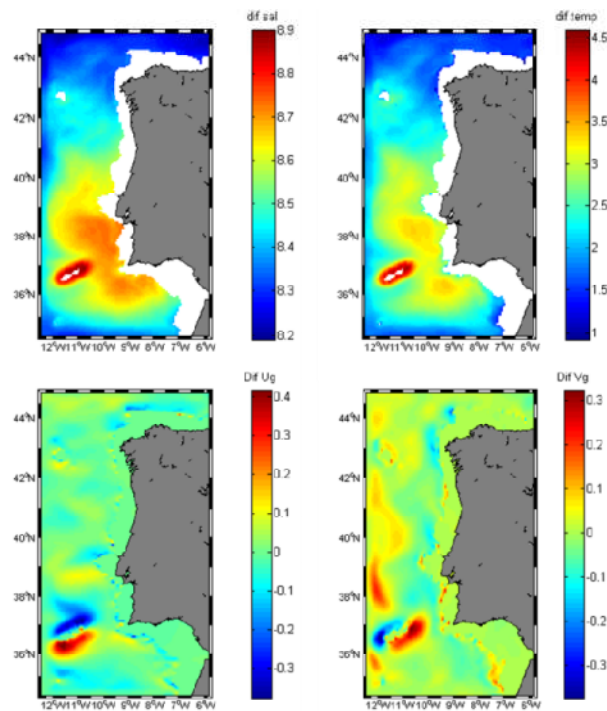


Figure 20: Comparison between annual climatology and the MOHID – model for salinity (upper left panel), temperature (upper right panel) and velocity fields U (lower left panel) and V (lower right panel) at 650m.

3. Comparison to the Mercator - model

The Mercator – data are interpolated to the grid used in this particular simulation, before we start calculating the monthly root mean square error for temperature and salinity and the biases in residual velocity. As Mercator does not incorporate a tidal module, it would be useless to compare instantaneous velocities. Instead, we compared residual velocities which we averaged over the depth – intervals of the pre – defined boxes described in chapter III.

At the surface, biases in temperature and salinity are mainly due to differences in bathymetry, river discharges and the fact that Mercator is forced by climatology whereas MOHID is forced by the Mercator – results. Temperature differences are generally larger than salinity differences due to the large temperature variability. Biases in residual velocity vary between -0.6 and 0.6 and are mostly due to the use of different bathymetries and MOHID’s strong relaxation at the boundaries. Nevertheless, there is a growing anomaly in residual velocity V around 41°N, which might indicate a larger westward transport of shelf waters by the MOHID – simulation.

At 100m of depth, biases in salinity are more pronounced at Cape St. Vincent. This might be explained by the fact that the slope current in the MOHID – simulation remains constrained to the slope, whereas the Mercator – results show more divergence around the cape. As the slope current diverges more in the Mercator – model, it will be subjected to a lot of mixing thus lowering its temperature. Consequently, the high bias in salinity is followed by a very distinct temperature bias along the slope between 37 and 39°N. The biases in temperature and salinity around 37.8°N are a result of the geostrophic current which carries warm, saline water into the region. This currents position is marked by a seasonal variation, as it depends on temperature and salinity fields. The larger bias in this region is therefore caused by the fact that Mercator is forced by Reynaud’s climatology while MOHID uses the Mercator – solution to force initial conditions.

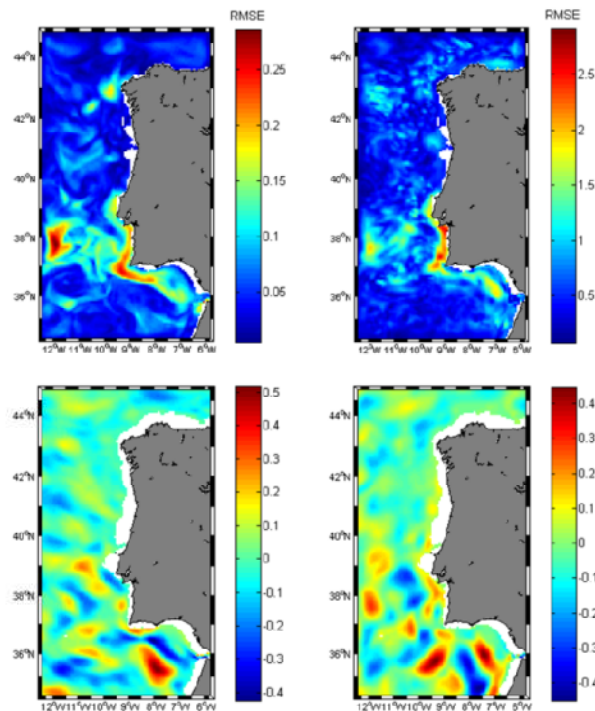


Figure 21: Root Mean Square Error in salinity (upper left panel) and temperature (upper right panel) and biases in residual velocities U (lower left panel) and V (lower right panel) between the Mercator and the MOHID – simulation for July 2006 at 100m of depth.

The bias in salinity at the Strait of Gibraltar at this level, might be less pronounced, but can not be ignored when comparing it to the differences in residual velocity U. In chapter III we already mentioned Mercator uses a strong relaxation to climatology in this region in order to better simulate the descent of Mediterranean waters into the Gulf of Cadiz. This strong relaxation to climatology leads to a very rapid descent which results in a negative bias in residual velocity U. Other biases in velocity are mostly due to the different bathymetries or to the strong relaxation of the MOHID – simulation.

At 250m the biases due to topography have become more pronounced, especially around the Gorringer seamount and in the vicinity of the Galicia bank. Furthermore, we also notice the more intense salinity anomaly in the Strait of Gibraltar as the sill is situated at about 360m. The temperature anomaly is situated more to the south, suggesting mixing at this depth already takes place in the Gulf of Cadiz.

At 650m the salinity anomaly remains south of 37°N and although the root mean square error varies only slightly between 0.45 and 0.50. The anomaly seems to be propagating itself along the shelf. This propagation can be explained by initial conditions; at first the model is initialized with zero velocity and then it continues its monthly calculations with the results of the previous month. The salinity bias due to Mercator's relaxation to climatology will therefore be propagated along the continental shelf. As there is a strong influence of Mediterranean waters on this level, the bias caused by the relaxation to climatology and initial conditions is more pronounced here. The temperature bias behaves similar to the salinity bias and varies between 0 and 2. It attains its highest values in January. Seasonal variation in the Gulf of Cadiz at this level is thus dominated by the variability of the Mediterranean water. The Mediterranean outflow is constituted of deep water masses which are formed by winter convection in the Gulf of Lions, hence its peak in winter.

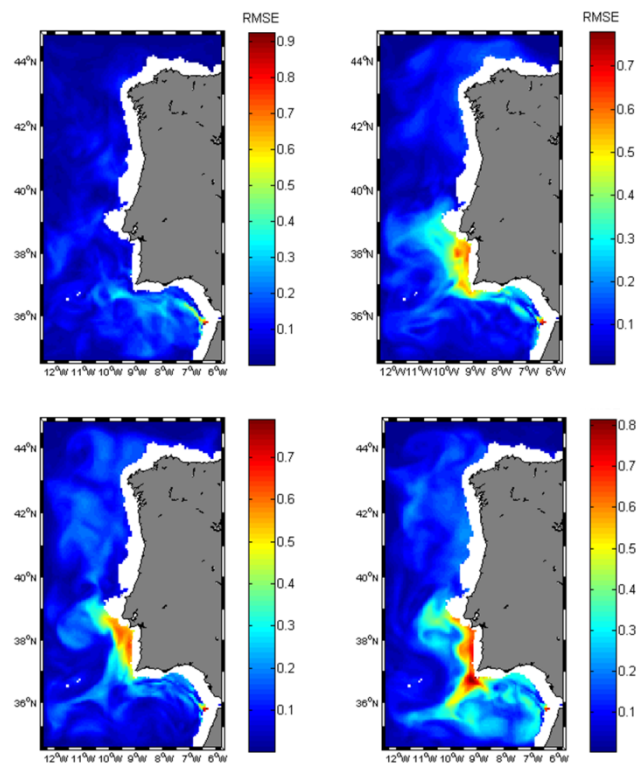


Figure 22: Root mean square error in salinity between the Mercator and the MOHID – model in August 2006 (upper left panel), October 2006 (upper right panel), December 2006 (lower left panel) and January 2007 (lower right panel).

As residual velocities decrease with depth, the differences between the Mercator and the MOHID – simulation are smaller. Nevertheless, the influence of the MOHID – relaxation at the western open boundary is clearly noticeable, especially for the meridional velocity. Most other biases are caused by topography and become more intense when main currents intensify, that is from August until November.

As expected, biases in velocity are even smaller at 1400m of depth and anomalies due to differences in topography are more pronounced. Root mean square errors in temperature and salinity do not display the same tendency, on the contrary they vary even more. These variations are due to the seasonality of the lower core of Mediterranean water which has a profound influence on the water masses at this level. Another interesting feature is the clearly defined large anti - cyclonic gyre at 38°N which separates offshore waters from shelf waters. As the gyre is slightly more pronounced in the Mercator – model, there exists a small positive bias in temperature and salinity. This gyre was already weakly present at 650m of depth (also see figure 4) and inhibits mixing from Mediterranean water with deep waters from Cape St. Vincent until the Tagus estuary.

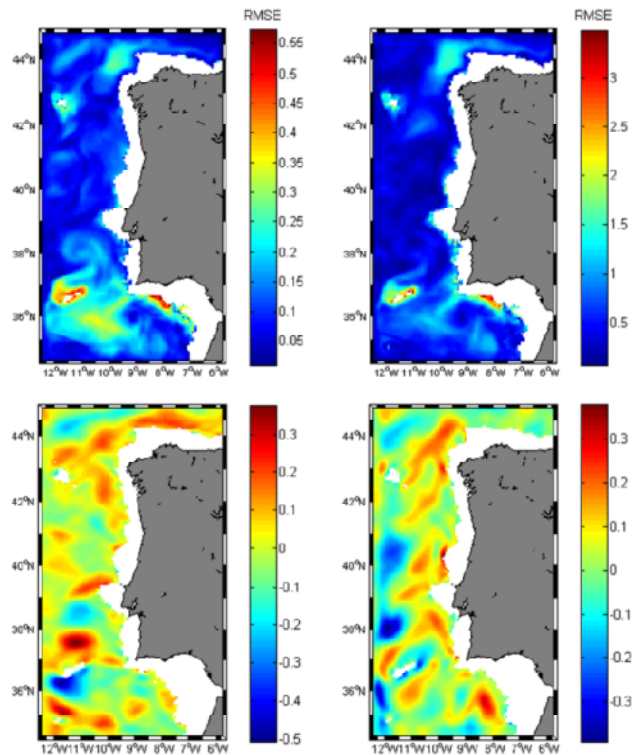


Figure 23: Root Mean Square Error in salinity (upper left panel) and temperature (upper right panel) and biases in residual velocities U (lower left panel) and V (lower right panel) between the Mercator and the MOHID – simulation for October 2006 at 100m of depth.

4. Validation with in situ – data

4.1 MORENA – campaign

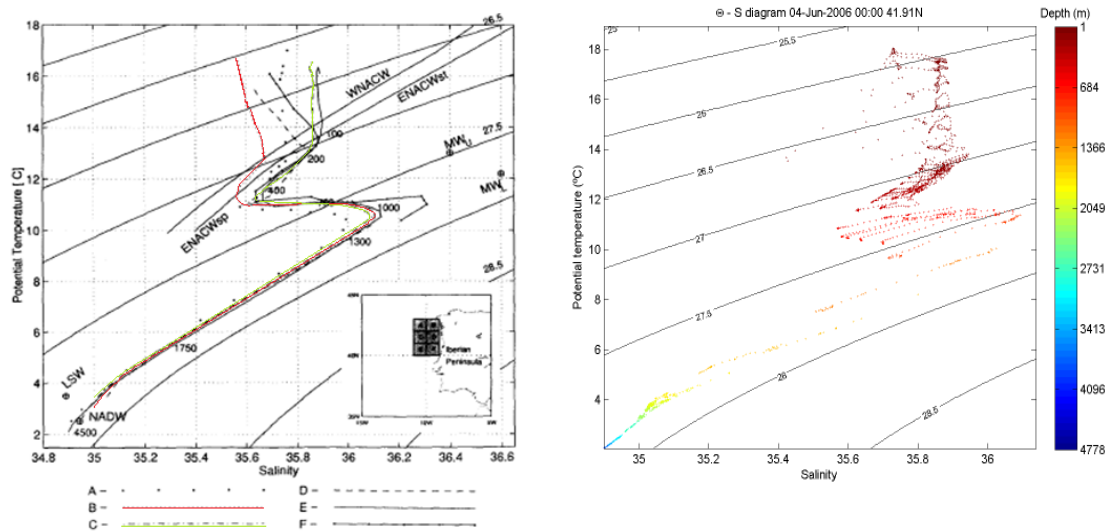


Figure 24: θ – S diagram of in situ data from the Morena campaign in May 1993 (left panel, green and red lines) and from the Mohid – model along the same transect at 41.91°N in June 2006.

The MORENA – campaign was aimed at measuring, understanding and modeling the shelf ocean of the northern Iberian Peninsula between 40 & 43°N. In order to obtain a better comprehension of alongshore exchanges, a CTD – survey was carried out in different sections in May 1993 (see insertion on fig.22 left panel). The red profile represents the CTD – measurements on the shelf, while the offshore measurements are represented by the green profile. The right panel of figure 24 is a θ – S diagram of the MOHID - simulation in June 2006. As we compare these diagrams, we notice the influence off the Douro river run – off in the surface layer of the MOHID – model. The salinity maximum at 250m which marks the lower limit of the ENACW_{st} is slightly more pronounced in the MOHID – model (35.9 to 35.7), but both diagrams still represent this water mass around $\sigma = 27$. The underlying salinity minimum of the ENACW_{sp} is also more saline (35.7 to 35.6). At about 1000m we find a clearly defined core of Mediterranean water which is marked by a salinity maximum at 36.1. The MOHID – simulation represents thus fairly well the characteristics of upper and intermediate water masses, although deep water masses are more diverged than in situ values.

4.2 Argo floats

Argo floats are hydrostatically balanced floats which are capable of changing their buoyancy. Once they are deployed, they will change their buoyancy and descend to their depth of hydrostatical equilibrium. Once they have obtained neutral buoyancy, the floats will drift for 9 days at a continuous depth of 1500m. Then, the float will descend to a depth of about 2000m and starts making continuous measurement of temperature, salinity and pressure during its ascent to the surface where it will send the collected data to a satellite.

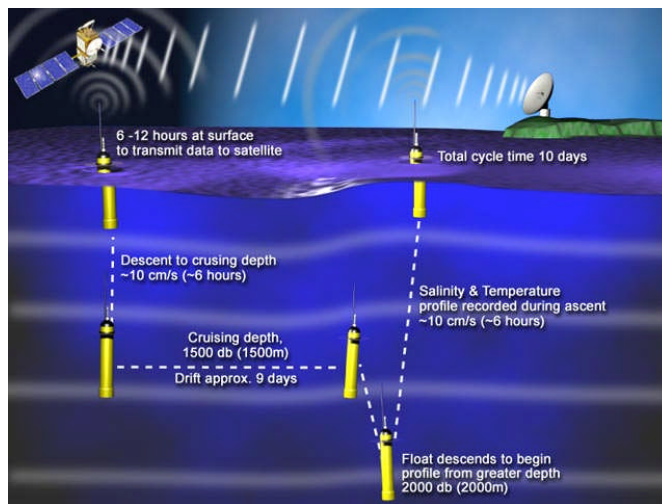


Figure 25: Description of an Argo mission
http://www.argo.ucsd.edu/ErHow_Argo_floats.html

As the Argo float is by nature a tool to map the deep ocean circulation, it is thus only useful to validate data in the deep ocean of the study region. Between June 1st 2006 and June 31st 2007, Argo - floats made 19 profiles in the study region. Most profiles were made in the north and the northwest of the study region between 42 & 45°N and 7 & 11°W. Some of these MOHID – profiles lie thus well within the models’ relaxation zone. Only 12 out of 19 profiles displayed both temperature and salinity profiles. The MOHID – data corresponds generally well to the in situ data with the exception of salinity of surface waters in stratified water columns and at intermediate depths where the model is less saline. The MOHID – profiles also display a linear evolution, whereas Argo – profiles are more curved as they represent a continuous data series.

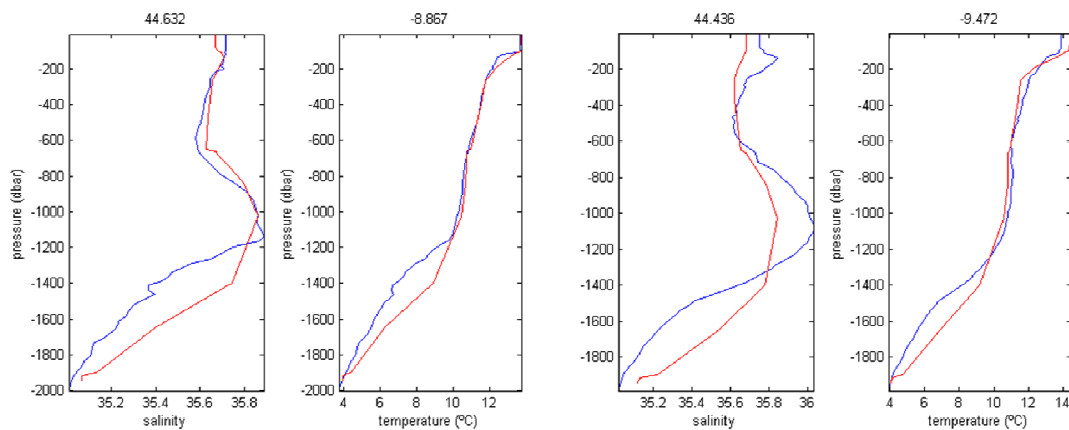


Figure 26: Argo - profiles (blue) and MOHID – profiles (red) on December 23rd 2006 (left panel) and January 1st 2007 (right panel). Positions are given by the coordinates in °N & °W above the profiles.

One example of the salinity bias in MOHID – profiles is given by the December 23rd and the January 1st profiles. As this bias is much smaller in other profiles with similar positions, the error must be due to the quality of the atmospheric data. The atmospheric data used to force the model in 2006 had only a seven day temporal resolution which was not as good as the three – daily atmospheric data used since February 2007. We should also notice that all Argo – profiles are made in the open ocean where the atmospheric model has a 27km spatial resolution. This salinity error in surface waters is thus entirely due to the quality of the input data. Consequently we should be very careful interpreting salinity profiles of the upper 250m of the water column anterior to February 2007. The MOHID temperature profiles on the other hand, seem to be corresponding

very well to the in situ data. They display a transition point at about 250m of depth which can be explained by the spatial discretisation of the simulation. As the vertical layers vary exponentially, the layer above 250m is much thicker than the layer just below 250m of depth (54m vs.11m). Consequently the MOHID – profiles are less accurate between 196 and 250m of depth. The same phenomenon is encountered at 650 and 1400m of depth, where it is even more pronounced as the overlying layer is thicker.

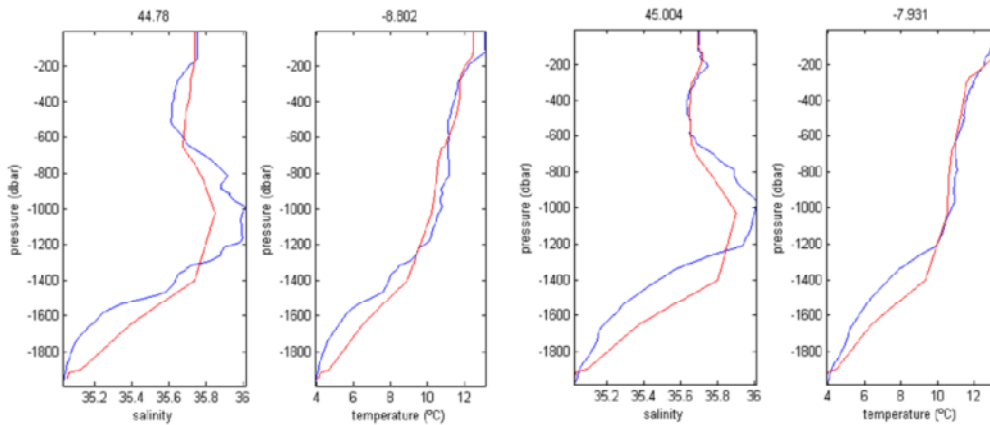


Figure 27: Argo - profiles (blue) and MOHID – profiles (red) on February 11th 2007 (left panel) and February 21st 2007 (right panel). Positions are given by the coordinates in °N & °W above the profiles.

At the level of the ENACW_{sp} and the WNACW, between 250 and 600m of depth, MOHID salinity data either corresponds well to the in situ data or it is more saline. If it is more saline, the data represent the characteristics of the ENACW_{sp}, which sometimes replaces the fresher WNACW in these regions. Therefore we can infer that the dynamics of the intrusion of WNACW in the north of the study region could be better represented in the model.

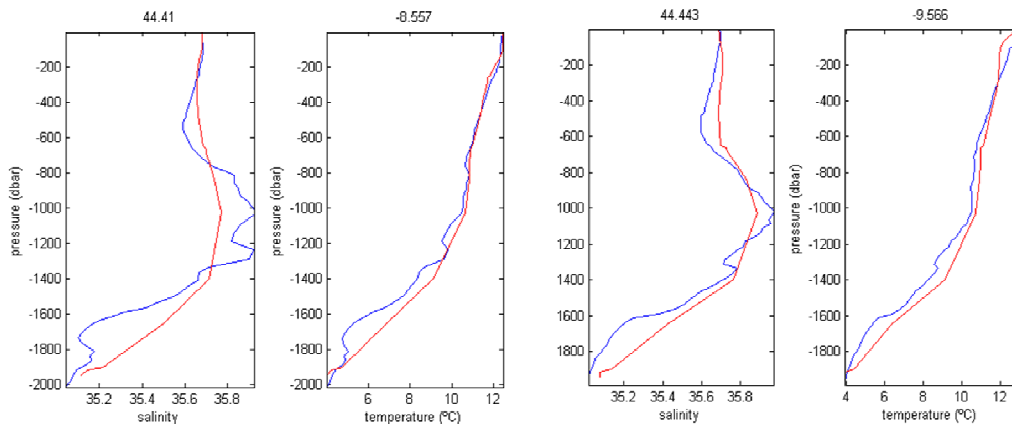


Figure 28: Argo - profiles (blue) and MOHID – profiles (red) on April 2nd 2006 (left panel) and April 12th 2007 (right panel). Positions are given by the coordinates in °N & °W above the profiles.

In intermediate waters, between 650 and 1400m of depth, temperatures correspond well, but Argo salinity is almost always superior to in situ data. This lack of salinity at the level of the Mediterranean waters can be due to an excessive vertical turbulent diffusion by the MOHID - model.

Between 1400 and 1900m of depth, the MOHID – profiles are very linear because of the thick vertical layers (250m). As the layers are less thick below 1900m of depth, all profiles will converge in deep waters.

5. Discussion

We can conclude that certain parts of the study region are more susceptible to display errors, e.g. the Mercator – relaxation zone to climatology will create large errors for temperature and salinity at intermediate levels and the relaxation of the simulation to barotropic velocities will create large biases in meridional velocity at the western open ocean boundary. Nevertheless, when comparing to the in situ data of the MORENA – campaign, we noticed that our data west off the Portuguese coast, between 40 and 43°N gives us a good representation of the characteristics of different water masses. The MOHID – data also fits fairly well the Argo – profiles made in the northeast and the northwest of the study region. In spite of that we should keep in mind that the 2006 salinity profiles in surface layers are less accurate due to the poor temporal resolution of atmospheric data. The lack of salinity in intermediate waters in this region is also something which should be looked into in order to obtain a better understanding of vertical diffusion and to improve its future parameterization. This validation of results has allowed us an insight into the errors of our simulation and can be used to obtain a good interpretation of results.

IV Results

1. Introduction

As validation has proven the model to give an acceptable representation of water properties and dynamics in the study region, we can now begin to analyze results. Nevertheless, we should always keep the most important findings of validation in mind whilst interpreting results. At first we shall try to deduce the changes in the main monthly circulation of the upper 1200m of the water column by analyzing the distribution of monthly temperature & salinity and residual velocities & volume transports. These residual volume transports through our pre – defined boxes are calculated over 24 days. Consequently, some of the sub – mesoscale features with a shorter timescale such as upwelling filaments and eddies might not be reproduced by these fluxes, rendering it very difficult to estimate the transport involved in the process. In the second part of this chapter we will try to demonstrate the occurrence of upwelling events in the region by studying meteorological data, twelve - hourly SST and monthly $\theta - S$ diagrams. The main problem in identifying these events is that, as they are very local and have a temporal timescale of only a few days, they might not be reproduced by the models' data which has a larger timescale.

2. Main circulation

2.1 Surface waters (0 – 100m)

The circulation in the surface layer is largely influenced by atmospheric forcing and river run – off and displays thus a strong seasonal variability. In July 2006, the equatorward component of the northeast trade wind is very weak and the surface circulation is predominantly northward. The largest poleward transport can be found at about 36°N & 10°W which carries 2.53 Sv of central and surface waters. A part of this warm, saline water is re - circulated in the Gulf of Cadiz. In the north of the region, we find an offshore poleward transport of 1Sv and on the shelf, the influence of the Western Iberian Plume totals 0.8 Sv.

By September, the large flux in the south will have increased to 3 Sv and it enters the region from the southwest. As northerly winds have become very strong by now, there is no offshore poleward transport. As a consequence, the mass of this flux will enter the Gulf of Cadiz and thus increase the flux of Atlantic water entering the Mediterranean. Offshore we find a large equatorward transport of 3.6 Sv. The geostrophical current which enters the region between 37 – 40°N is only weakly present and seems to be subdued by the equatorward currents. In fact, the entire circulation in the study region seems to be dominated by the geostrophical and by equatorward currents due to northerly winds. In late autumn and early winter, the geostrophical current intensifies to 3Sv and becomes the dominant feature in the study region south of 39°N. It meanders south and re-enters the region in the southwest supplying the Gulf of Cadiz with 1Sv of warm, saline waters and feeding the weakened poleward current that totals 0.8 Sv. In January, northerly winds become dominant, forcing the geostrophic current to the south and thus reducing its contribution to 1.6 Sv. In the north we already observe an offshore equatorward transport of 1.2 Sv. March is characterized by a transient regime with a weak offshore equatorward transport of 0.3 Sv and a large geostrophic inflow into the Gulf of Cadiz (2.5Sv). By May, this geostrophic inflow has totally disappeared and off Cape St. Vincent we find an equatorward flow of 2 Sv. This equatorward flow is already reversed into a poleward of 1.8 Sv in June, indicating the great variability of fluxes in summer.

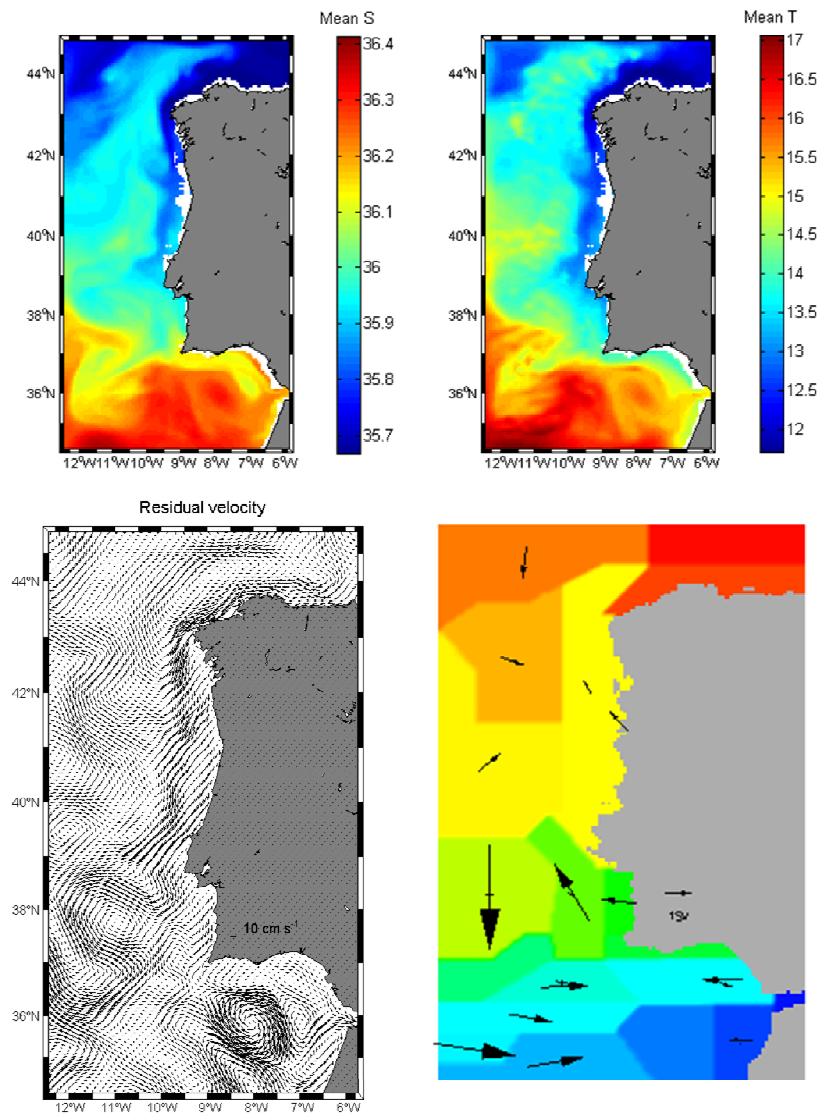


Figure 29: Monthly mean temperature and salinity, and residual velocity and volume transport for surface waters in September 2006.

2.2 Subtropical central waters (100 – 250m)

Transports in tropical central waters are generally much smaller than transports in the surface layer, since they are not subjected to atmospheric forcing and experience a lot more friction from overlying and underlying water masses. At this level, the geostrophic current is mainly constituted of $ENACW_{st}$ is also more prominent. In July 2007, all features are nearly the same as those in surface layers with 0.5Sv entering into the Gulf of Cadiz, an offshore poleward flow of 0.3 Sv and over the shelf, 0.7Sv of the Western Iberian Plume. All but one feature, because in the north there is an intrusion of WNACW by a meandering equatorward current which totals 0.4Sv. These WNACW are separated from the $ENACW_{st}$ by the Galicia front. In September the geostrophic current is (0.286 Sv) deviated to the south by an equatorward current off Cape St. Vincent of 0.342 Sv. This pattern is consistent with the main features in the surface layer and is thus a downward extension of the surface circulation. In late autumn and early winter, both equatorward and geostrophic current are intensified intermittently (1 Sv vs. 0.75 Sv). The geostrophic current is meandering strongly and re – enters the

region in the south to contribute another 1 Sv to the Gulf of Cadiz. After that, the equatorward current takes over and pushes the geostrophic current to the south resulting in an equatorward current in the north of 0.85 Sv and one off Cape St. Vincent of 0.75Sv. Meanwhile both geostrophic contributions quantify only 0.25 (at 38°N) and 0.6 SV (in the south) respectively. In February the geostrophic current becomes again dominant, only to lose its influence to the equatorward current in the north of the region in March. We also observe tropical central waters rounding Cape St. Vincent, rather than re-circulating offshore before continuing their poleward current. This can thus be seen as the onset of the poleward slope current in subtropical central waters.

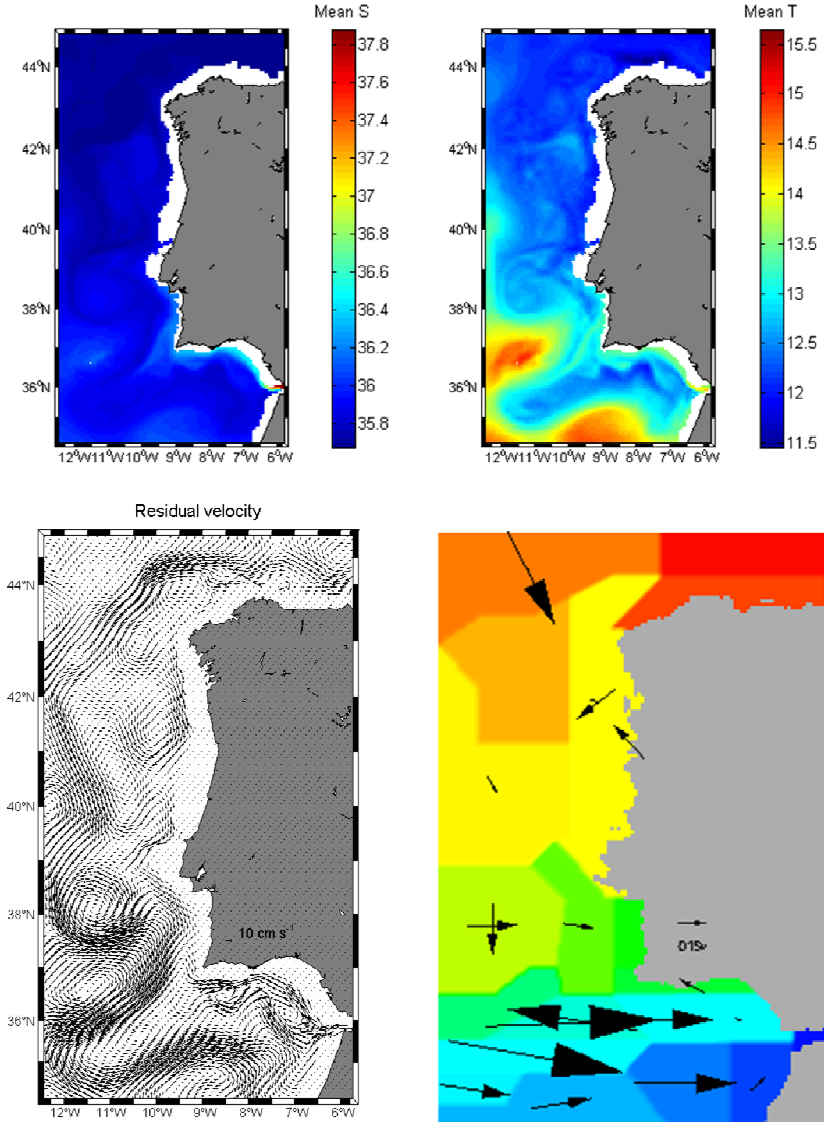


Figure 30: Monthly mean temperature and salinity, and residual velocity and volume transport for March 2007 in subtropical central waters

In May, both the geostrophic and the equatorward current gain force (0.68 vs. 1.42 Sv), but the equatorward seems to gain as it deviates the geostrophic current to the south. June on the contrary is marked by a transient regime in which fluxes at 38 °N are almost equal (0.5 for the equatorward current vs. 0.6 for the geostrophic current). In such a situation, the region north of 38°N will be dominated by the equatorward flux, while the region to the south is under the influence of the geostrophic flux of ENACW_{st}.

2.3 Subpolar central waters (250 – 650m)

In July, subpolar central waters in the south of the region are marked by a weak, offshore poleward flow of 0.15 Sv and a rather large eastward geostrophic current of 0.6Sv. The north is dominated by a southwestward intrusion of WNACW and an offshore poleward current of 0.53Sv. September on the other hand is a month with a very intense circulation resulting in an offshore equatorward current of 0.5Sv at 40°N and a smaller poleward current along the slope (0.25Sv) at the same latitude. Further, we also find a well defined equatorward current in the north (0.43Sv), meandering south and producing another flux (0.25Sv) at 40.5°N.

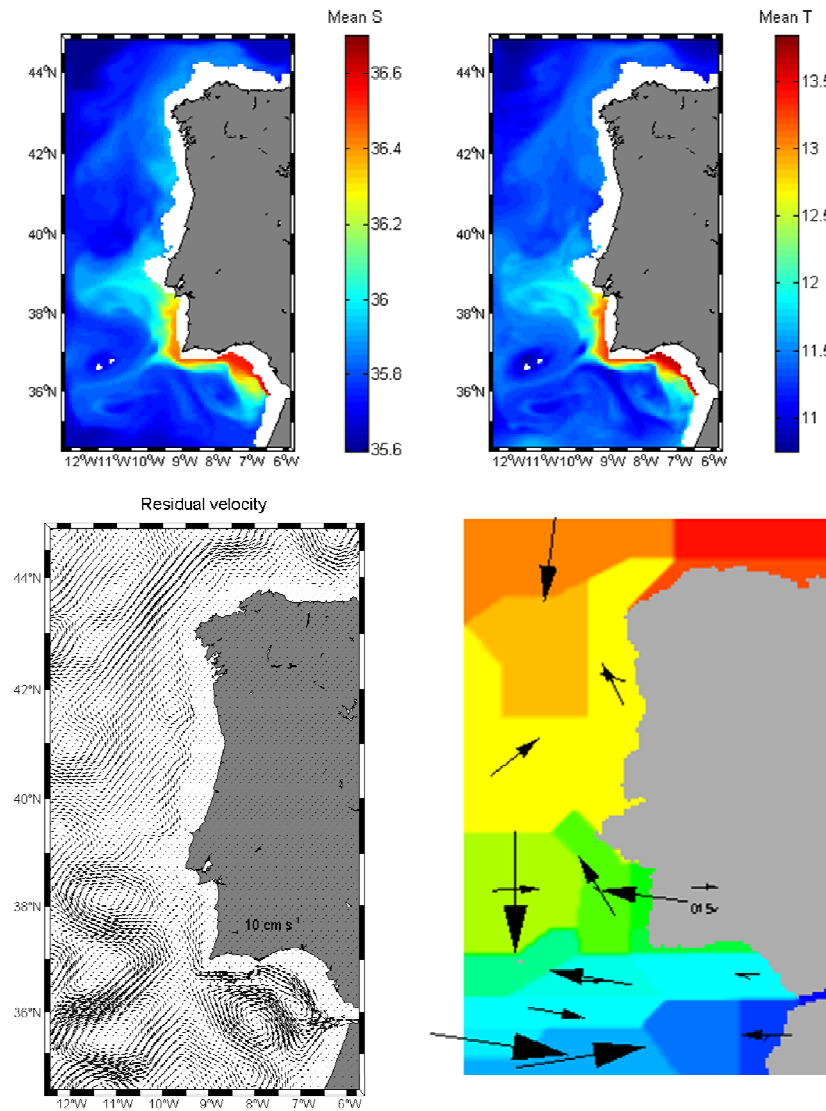


Figure 31: Monthly mean temperature and salinity, and residual velocity and volume transport for September 2006 in subpolar central waters.

In October 2007, circulation is largely to the south (1.27 Sv at 41°N) and north of the Galicia front at 42°N., large fluxes of WNACW enter the region (0.9 and 0.6 Sv respectively). This southerly circulation pattern is already overthrown by a strong geostrophic circulation of 0.95 Sv by November. As this geostrophic current meanders and re – enters the region it contributes another 1.18 Sv to the region of which 0.27 Sv supposedly enters into the Gulf of Cadiz. If we compare the residual volume

fluxes to the residual velocities, we notice that the flow entering the Atlantic through the Strait of Gibraltar is not always represented by the volume fluxes (also see circulation at 250m in the electronic appendix). This is because the model considers that this flux is coming from a place outside its predefined boxes. Such fluxes are referenced as coming from box “zero” which is the box that contains all fluxes which do not belong to one of our boxes. In order to represent this fluxes, box “zero” is said to re – group the entire domain and as fluxes originate from the geometrical boxes, this should create a very confusing knitting of arrows all over our figure. These arrows are thus suppressed by the routine used to produce manageable output files.

Meanwhile, in the north of the region, offshore circulation remains equatorward with a transport of 0.95 Sv, while 0.63 Sv is transported northward along the continental slope. By January, the circulation has become predominantly equatorward again, with large fluxes of WNACW (3.05 Sv and further south 0.98Sv) opposed to a weak geostrophic flow (0.25Sv). This circulation pattern remains dominant until April, when the geostrophic current enters the region again and uses its transport of 0.52 Sv as a wedge to separate its large meanders in the southwest of the region (1.42 Sv and 0.92 Sv respectively) from the fluxes of WNACW in the north (0.52 and 0.66 Sv). Consistent with observations in overlying layers, this last circulation is subdued by June, as the equatorward circulation gains in force (0.7sv vs. 0.64 Sv).

2.4 Intermediate waters (650-1200m)

In intermediate waters, the dominant water mass consists of Mediterranean waters, although in the northwestern part of the region significant volumes of Labrador Sea Water can be present. This Labrador Sea Waters are almost never found south of about 42°N, as there is a downward extension of the Galicia front which separates them from water masses in the south. This extension is marked by a strong salinity gradient between LSW and MW.

In late summer, circulation in the north is mostly poleward or eastward and fluxes vary from 2 to 4 Sv. In the south of the region, the geostrophic current varies between 0.75 and 1.2 Sv as it calmly re – circulates in the Gulf of Cadiz. By September, circulation in the north has become equatorward (1Sv) and the poleward current only persists along the slope (0.8Sv). In the south we can also find an offshore, equatorward flux (0.3Sv) and a poleward transport along the slope of the Lisbon Promontory (0.67Sv). In October this equatorward circulation pattern intensifies to be overturned by a large wedge of geostrophic flow (2.5 Sv) in November. This concurs well with events in surface layers and it is thus likely that not only Mediterranean waters have a profound influence on surrounding waters, but that surface waters can also influence circulation on an intermediate level. By December, the equatorward flux at 38°N has increased to 1.11 Sv and it has pushed a large part of the original geostrophic flow south. The latter has increased again during December, turning the system around into a transient regime between dominating equatorward or geostrophic flow. In January, the equatorward flow (2Sv and 3.3 Sv for the northerly LSW) seems to have won as circulation is mostly south except for the most southern waters where some meanders of the geostrophic current can persist.

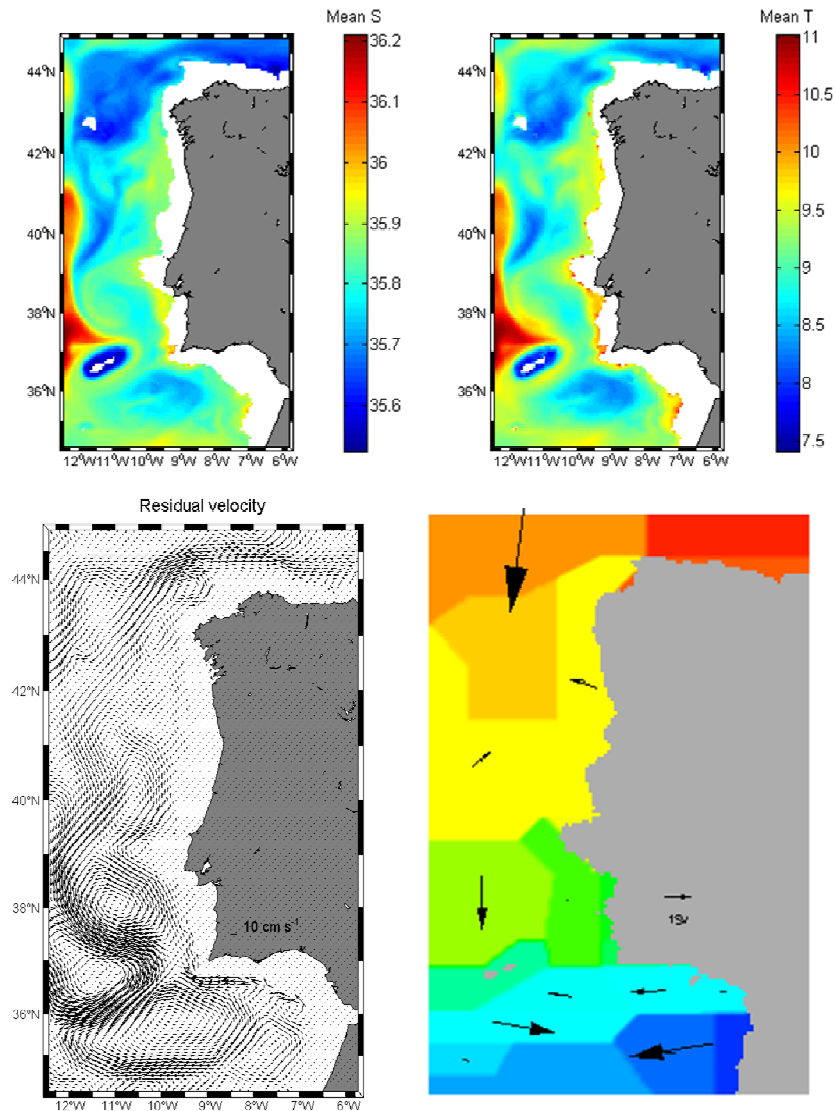


Figure 32: Monthly mean temperature and salinity, and residual velocity and volume transport for January 2007 in subpolar central waters.

Although the geostrophic current at 38°N is not re – established by February, circulation becomes almost entirely eastward with the largest fluxes in the southwestern part of the region (2.08 & 2.5 Sv). In April, the geostrophic circulation at 39°N is re – established and we can even find a poleward current (1.3 Sv) at 36 °N and the poleward current in the north now totals up to 1.92 Sv. In May this poleward current has transformed into a countercurrent (4.1 Sv) by a strong equatorward current at 44°N (1.75 Sv). By May, circulation is again predominantly south.

3. Upwelling events

3.1 Introduction

As the Iberian Peninsula has an east – west and a north – south orientated coast, upwelling prerequisites will be different. Furthermore, the presence of capes will enhance the offshore transport of shelf waters and so stimulate upwelling. Besides that, these topographical features also force all water masses thus rise, which avoids a well stratified water column. Along the north – south coast upwelling occurs under northerly winds. These winds are largely influenced by the position of the Azores high and consequently they should be more frequent and intense when the Azores High moves northward in summer.

3.2 West – coast of Portugal

Upwelling events along the Portuguese West coast always begin with northerly winds at about 44°N, as the winds persist, the upwelling will spread further south. By analyzing MOHID's 12 hourly SST – fields we found the upwelling events described in table 1.

| Date | Δ Temperature | Δ SST over 100km | Zonal wind stress τ from MM5 | Ekman transport per 100m of coast |
|-------------------------|----------------------|-------------------------|-----------------------------------|-----------------------------------|
| 14 – 18 /07/ 2006 | 14 – 17 °C | -3 | -0.17303984 | -16.69286 |
| 28/07/2006 – 01/08/2006 | 16.1 – 18°C | -1.9 | Lacking MM5 data | |
| 8 – 23/08/2006 | 16 – 18 °C | -2 | -0,10996419 | -10.60807 |
| 29/08/2006 - 03/09/2006 | 15 – 17.4°C | -2.4 | -0,0248840 | -2.40052 |

Table 1: Periods of upwelling events, minimum and maximum temperature 100 km apart at the same latitude at the beginning of the upwelling event, the resulting Δ SST over 100km zonal wind stress and Ekman – transport

If we want a simple estimation of the transport induced by the upwelling, we can suppose a steady state and an invariable zonal wind stress. Then we can apply the following formula:

$$UI = \frac{\tau m^3}{\rho f s} / 100m$$

With f the Coriolisparameter and ρ the water density (Kundu, 3rd edition). If we multiply the smallest transport by the maximum length of the upwelling zone, we obtain a value of 0.2 Sv which is entirely consistent with the value of Mazé (1997) in chapter II.

3.3 Cape St. Vincent

Instead of watching endless fields of SST – data, we can also make transects of MOHID – data at the capes and use these data to construct monthly $\theta - S$ diagrams. Figure 31 provides us with these data at Cape St Vincent, in the south of Portugal. As the wind is very variable and strong in autumn, profiles are much dispersed. Once the winds are constantly coming from the south in winter and once they have weakened, the profiles become remarkably stratified.

At Cape St. Vincent, upwelling is normally induced in late spring and early summer by westerly winds, but unfortunately, the model data represented only a very weak signature of this feature.

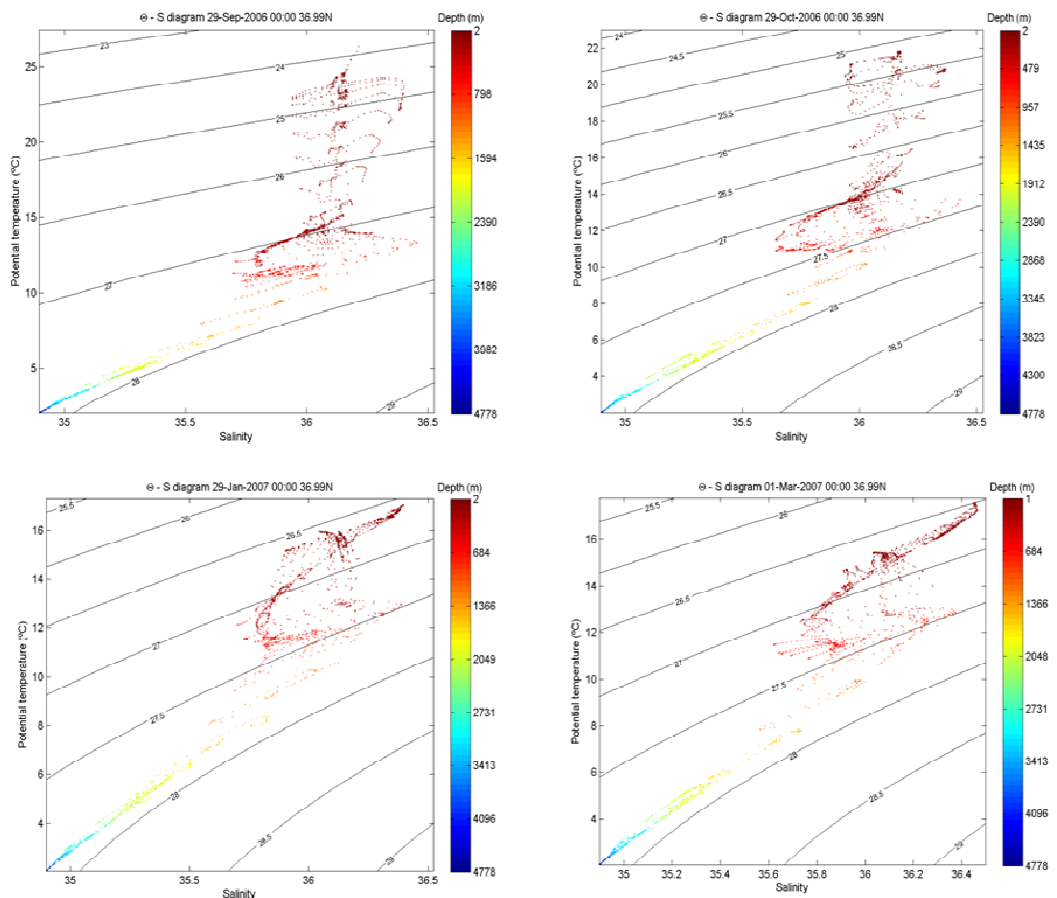


Figure 31: Monthly $\theta - S$ diagrams at 36.99°N for September 2006 (upper left panel), October 2006 (upper right panel), January 2007 (lower left panel) and March 2007 (lower right panel).

4. Discussion

In general, residual volume fluxes are well explained by the distribution of residual velocities, which reassures us of the quality of the spatial discretisation. In surface waters, we notice the influence of the WIBP over the shelf and the influence atmospheric forcing. Atmospheric forcing is largest in case of northerly winds, when an equatorward current in the north is able to overturn the initial poleward circulation. In fact, the entire system seems to be governed by this equatorward flow in the north and a geostrophic current which enters the region at 38°N. When northerly winds weaken in late autumn, this geostrophic current will wedge itself between the equatorward current and the currents south of 38°N, thus creating two subsystems. One in the north which in transient regimes might still display an southerly tendency under the influence of the equatorward current and one in south, governed by the geostrophic current. If the geostrophic current further increases in volume, its recirculation in the Gulf of Cadiz will be able to round the cape and form a poleward current along the continental slope. In some cases, the geostrophic current even succeeds in overturning the offshore equatorward circulation. If the equatorward current is prevalent (which is the case in the period January – March), it will deviate the geostrophic current to the south and circulation as far south as Cape St. Vincent will be predominantly southward. From March to April the system displays a transient regime, with an equatorward current governing the region north of 38°N and a dominating geostrophic current in the south.

Circulation at the level of subtropical central waters concurs well with circulation in surface waters. In the north of the region the ENACW_{st} is separated from the WNACW by the Galicia front. When the equatorward regime becomes dominant, this east – west orientated front can be found at 42°N, its most southerly latitude. This Galicia front thus forms an interruption of offshore equatorward current or the poleward current under geostrophic regime. As a consequence the equatorward and the geostrophic current will start meandering, leaving and re – entering the study region. The position of the Galicia front is thus a good indication of the governing regime. At the level of the subpolar central waters, circulation is very similar to the circulation in subtropical central waters. We also notice a lack of representation in residual volume fluxes of the Mediterranean flow entering the Atlantic. This is because such a flow is considered to come from box “zero” outside the models’ domain. The centre of this “zero” boxes is taken to be the geometrical centre of the entire domain and representation of fluxes from box “zero” would thus result in a very confusion knitting of fluxes all over the figure.

In intermediate waters we find a downward extension of the Galicia front in the form of a salinity gradient between the more saline Mediterranean waters and the Labrador Sea Water. This downward extension will display the same dynamics as the Galicia front, which proves Mediterranean waters do not only influence surrounding waters, they can also be influenced by surface waters. Although there are only very few studies on volume transports, our values of 0.55 Sv in surface waters and 0.8Sv in intermediate waters for the poleward current over the shelf correspond well to Stevens’ total value of 1.2 Sv (Stevens & al.,2000)

As residual volume fluxes between our pre – defined boxes are calculated over 24 days, some sub – mesoscale features with shorter timescales such as upwelling events are not represented by these fluxes. Therefore we analyzed meteorological data, surface SST and $\theta - S$ diagrams to identify these phenomena. As the number of events for our simulation period is very low, we can satisfy ourselves by quickly comparing our estimated transports to the values found by Mazé (1997).

V Conclusion

The Iberian system is an extremely interesting system in the sense that it not only displays a strong seasonal variability, but also is subjected to the influence of a lot of sub - mesoscale features. The seasonal variability is caused by the migration of the Azores High. In summer, the Azores High migrates north and induces equatorward surface currents. In winter, the Azores high migrates back south and the system is characterized by a poleward circulation. Although Fúza (1982) defined the period of northerly winds as April – October, our simulation also displays equatorward currents in January – March as a consequence of atmospheric forcing. This inter - annual discrepancy might be explained by a variation in the North – Atlantic Oscillation, but as we only simulate for the period between June 1st 2006 and June, 26nd 2007, the variability of the NAO goes beyond the scope of our study. As we carried out a thorough validation of results we are re – assured of the quality of our data. Most discrepancies that arose during the validation with the Mercator – model were due to the differences in initial or boundary conditions or to the use of different bathymetries. Validation with the in – situ '93 data of the MORENA – campaign have shown MOHID is capable of accurately reproducing the characteristics of the main water masses of the Iberian system. The small biases in salinity in surface layers we found while comparing with Argo – data were entirely due to the poor temporal resolution of the atmospheric data we introduced into the model. The salinity bias at intermediate levels is explained by the models' parameterization of vertical diffusion which is somewhat overestimated.

The volume fluxes calculated to quantify the variability of water masses west off the Iberian Peninsula coincide well with the distribution in residual velocities, which proves that the spatial discretisation we introduced into the model is adequate. In surface and intermediate waters, the entire system is dominated by either an equatorward or poleward circulation except for the poleward current over the shelf. Although this poleward slope current is less subjected to the changes in wind direction, it might be overturned in surface layers.

In summer the system is dominated by equatorward flows as a result of northerly winds. These winds weaken in late autumn northerly winds weaken and the system is divided into two subsystems: one north of 38°N governed by an equatorward flow and one in the south dominated by the geostrophic current. At the level of the subtropical and the subpolar central waters, we notice the presence of the Galicia front at 42°N. This front separates the eastern central waters from the denser western central water masses and it even has a downward extension at intermediate levels where it is being reinforced by the salinity gradient between LSW and Mediterranean waters. The position of the fronts sometimes forces the equatorward and the geostrophic current to leave the study region, meandering and re – entering at the western boundary. From January until March the equatorward currents are prevalent again. In March – June the system displays a transient regime with an equatorward current in the north and a geostrophic current in the south trying to overturn the other current.

The lack of representation of the Mediterranean Outflow through the Strait of Gibraltar is the result of a particularity of the post – processing routine. All fluxes coming from outside the domain are represented as originating in box “zero”, this box is centered at the geometrical centre of domain. A representation of these fluxes would thus lead to a confusion knitting of fluxes all over the figure. Therefore we have chosen not to represent these fluxes.

As there have been only a few studies on the quantification of transports in the Iberian system, we can only compare our values of 0.55 Sv in surface waters and 0.8 Sv in intermediate waters to the poleward slope currents described by Stevens (2000), which totals 1.2 Sv. As residual fluxes between our – pre defined boxes are calculated over 24 days, they do not represent sub – mesoscale features such as upwelling events, which are responsible for most vertical transports. Therefore we studied 12 – hourly surface SST, monthly $\theta - S$ diagrams and meteorological data in order to identify these events. As they are not frequent, we satisfy ourselves by comparing the smallest of our estimated transports to the transports described by Mazé (1997).

Taking into account all these observations, we can conclude we succeeded in providing a reasonable approximation of transports of different water masses west of the Iberian Peninsula. As there is very little literature on this subject, we intend to publish an article that contains our data. Future studies on this subject should be carried out at a greater timescale in order to demonstrate inter - annual and variations caused by the NAO. It might also be useful to reduce the temporal timescale at which residual volume fluxes are calculated to obtain a better estimation of upwelled transports, but this should seriously increase the model's calculation cost.

List of figures

Figure 4 p.4: Bathymetry of the study region with the main topographic features

Figure 5 p.5: Examples of salinity and temperature profiles obtained in the north (45°N14°W, lower panel) and south (40°N,12°W, upper panel) surface waters (Fiuza & al., 1998).

Figure 6 p.6: $\theta - S$ diagram of water masses off the Iberian Peninsula during May 1993 (Fiúza et al.,1998)

Figure 4 p.7: The Portugal current system in January-March, in May-June, in July-Sept and in Oct.-Dec <http://oceancurrents.rsmas.miami.edu/atlantic/portugal.html>

Figure 5 p.8: Distributions of temperature and salinity at 10dbar (Fiúza et al., 1998).

Figure 6 p.9: Thickness of the layer of ENACW_{st}, % of Azores Mode Water in the ENACW_{st}, the geopotential anomaly at 200 dbar relative to 350 dbar (Fiúza et al., 1998).

Figure 7 p.10: Pathways of Mediterranean water as observed by AMUSE (Bower & al., 2002)

Figure 8 p.11: Percentage distributions of the different water masses and thermohaline characteristics of the deep layer at 1800 dbar (Fiúza & al., 1998)

Figure 9 p.12: Wind, Ekman transport and Ekman transport per degree of latitude calculated by Mazé & al., 1997.

Figure 10 p.14: Schematic overview of the MOHID - model

Figure 11 p.15: Horizontal and vertical boxes used in this MOHID simulation

Figure 12 p.16: Mean daily Douro temperature and a polynomial of the fifth degree

Figure 13 p.17: Schematic overview of the MM5- weather forecast model

Figure 14 p.20: Total kinetic energy of the simulation

Figure 15 p.21: Relaxation zone of the MOHID - model

Figure 16 p.21: Sponge layer of the MOHID - model

Figure 17 p.22: The Arakawa C grid

Figure 28 p.23: Leendertse discretisation of a semi - implicit ADI scheme

Figure 19 p.25: Comparison between annual climatology and the MOHID – model for fields of salinity (upper left panel), temperature (upper right panel) and velocity fields U (lower left panel) and V (lower right panel) at 8m of depth.

Figure 20 p.26: Comparison between annual climatology and the MOHID – model for salinity (upper left panel), temperature (upper right panel) and velocity fields U (lower left panel) and V (lower right panel) at 650m.

Figure 21 p.27: Root Mean Square Error in salinity (upper left panel) and temperature (upper right panel) and biases in residual velocities U (lower left panel) and V (lower right panel) between the Mercator and the MOHID – simulation for July 2006 at 100m of depth.

Figure 22 p.28: Root mean square error in salinity between the Mercator and the Mohid – model in August 2006 (upper left panel), October 2006 (upper right panel) , December 2006 (lower left panel) and January 2007 (lower right panel).

Figure 23 p.29: Root Mean Square Error in salinity (upper left panel) and temperature (upper right panel) and biases in residual velocities U (lower left panel) and V (lower right panel) between the Mercator and the MOHID – simulation for October 2006 at 100m of depth.

Figure 24 p.30: $\theta - S$ diagram of in situ data from the Morena campaign in May 1993 (left panel, green and red lines) and from the Mohid – model along the same transect at 41.91°N in June 2006.

Figure 25 p.31: Description of an Argo mission, http://www.argo.ucsd.edu/FrHow_Argo_floats.html

Figure 26 p.31: Argo - profiles (blue) and MOHID – profiles (red) on December 23st 2006 (left panel) and January 1st 2007 (right panel). Positions are given by the coordinates in $^{\circ}\text{N}$ & $^{\circ}\text{W}$ above the profiles.

Figure 27 p.32: Argo - profiles (blue) and MOHID – profiles (red) on February 11th 2007 (left panel) and February 21st 2007 (right panel). Positions are given by the coordinates in $^{\circ}\text{N}$ & $^{\circ}\text{W}$ above the profiles

Figure 28 p.32: Argo - profiles (blue) and MOHID – profiles (red) on April 2nd 2006 (left panel) and April 12th 2007 (right panel). Positions are given by the coordinates in $^{\circ}\text{N}$ & $^{\circ}\text{W}$ above the profiles.

Figure 29 p.35: Monthly mean temperature and salinity, and residual velocity and volume transport for surface waters in September 2006.

Figure 30 p.36: Monthly mean temperature and salinity, and residual velocity and volume transport for March 2007 in subtropical central waters

Figure 31 p.37: Monthly mean temperature and salinity, and residual velocity and volume transport for September 2006 in subpolar central waters.

Figure 32 p.39: Monthly mean temperature and salinity, and residual velocity and volume transport for January 2007 in subpolar central waters.

Figure 31 p.41: Monthly $\theta - S$ diagrams at 36.99°N for September 2006 (upper left panel), October 2006 (upper right panel), January 2007 (lower left panel) and March 2007 (lower right panel).

Table 2 p.40: Periods of upwelling events, minimum and maximum temperature 100 km apart at the same latitude at the beginning of the upwelling event, the resulting ΔSST over 100km zonal wind stress and Ekman – transport

References

Books :

Kundu, P. and Kohen, I.,2004.Fluid Mechanics, Elsevier Academic Press, third edition

Courses:

Barth, A., 2008,Structure des modèles hydrodynamiques, Université de Liège

Beckers, J.–M., 2007, Mécanique des fluides géophysiques, Université de Liège

Doctoral theses:

Coelho,H.,2001,Modelação de Processos Físicos Relacionados com a Circulação Oceânica na Margem Continental Ibérica, Ph.D.thesis in environmental engineering, IST – UTL

Leitão, P. ,2002, Integração de Escalas e de Processos na Modelação do Ambiente Marinho, Ph.D.thesis in environmental engineering, IST – UTL

Master theses:

Sousa,T.,2002, Prévisão Meteorológica em Portugal Continental utilizando o modelo operacional de investigação MM5, Master thesis in ecology, management and modelisation of marine resources, IST–UTL

Articles:

Ambar, I. , Serra, N., Dias, J. & Relvas, P.,Theme 1 – Oceanographic Characteristics of the area, NE Atlantic Area off West and South Iberian Peninsula

Blayo, E. and Debreu, L.,2005,Revisiting open boundary conditions from the point of view of characteristic variables, Ocean Modelling, Vol.9, p.231–251

Bower,A., Serra,N. & Ambar, I.,2002, Structure of the Mediterranean Undercurrent and Mediterranean Water spreading around the southwestern Iberian Peninsula, Journal of Geophysical Research, Vol.107

Delhez, E. & Deleersnijder, E.,2007, Overshootings and oscillations caused by biharmonic mixing Ocean Modelling, Vol. 17, p.183–198

Drillet, Y. , Bourdallé–Badie, R. , Siefridt, L. & Le Provost, C.,2005, Meddies in the Mercator North Atlantic and Mediterranean Sea eddy – resolving model, Journal of Geophysical Research, Vol.110

Fiúza,A, Macedo,M.& Guerreiro, M.,1982, Climatological space and time variation of the Portuguese coastal upwelling, Oceanologica Acta,5,p.31 – 40

Fiúza, Hamann, Ambar, Díaz del Río, González & Cabanas,1998,Water masses and their circulation off Western Iberian during May 1993, Deep Sea Research I, Vol. 45, p.1127 – 1160

Holland, W. , Chow, J. and Bryan, F. ,1998, Application of a third order upwind scheme in the NCAR Ocean model, Journal of Climate, Vol.11, p.1487–1493

Hutchance, J., Van Aken, H., White, M., Barton, E., Le Cann, B., Ferreira, E., Alvarez, E., Miller, P. & Vitorino, J., 2002, Ocean Margin exchange – water flux estimates, *Journal of Marine systems*, Vol. 31, p.107 – 137

Juliano, M. & Alves, M., 2007, The Atlantic Subtropical Front/Current Systems of Azores and St. Helena, *Journal of Physical Oceanography*, Vol.37, p.2573–2598

Lyard, F., Lefevre, F. and Letellier, T., 2006, Modelling the global ocean tides, modern insights from FES2004, *Ocean Dynamics*, Vol.56, p.394 – 415

Marchesiello, P., McWilliams, J. and Shchepetkin, A., 2001, Open boundary conditions for long-term integration of regional oceanic models, *Ocean Modelling*, Vol.3, p.1–20

Marta-Almeida, M. and Dubert, J., 2006, The structure of tides in the Western Iberian region, *Continental Shelf Research*, Vol.26 (3), p.385–400.

Mazé, J., Arhan, M. & Mercier, H., 1997, Volume budget of the eastern boundary layer off the Iberian Peninsula, *Deep Sea Research I*, Vol.44, p.1543–1574

Peliz, A., Rosa, T., Miguel, A., Santos, P. & Pissarra, J., 2001, Fronts, jets and counter – flows in the western Iberian upwelling system, 2001, *Journal of Marine systems*, Vol.35, p.61 – 77

Pietrzak, J., Jakobson, J., Burchard, H., Vested, H. & Petersen, O., 2002, A three – dimensional hydrostatic model for coastal and ocean modeling using a generalized topography following coordinate system, *Ocean Modelling*, 4, p.173–205

Relvas, P., Barton, E., Dubert, J., Oliveira, P., Péliz, A., da Silva, J. & Santos, M., 2007, Physical oceanography of the western Iberia ecosystem: Latest views and challenges, *Progress in Oceanography*, Vol.74, p.149–173

Riflet, G., Leitão, P., Fernandes, R. & Neves, R., 2007, A simple pre-operational model for the Portuguese coast, CMNE/CILACME

Stevens, I., Johnson, J. & Fiúza, A., 2000, Comparisons between a fine resolution model and observations in the Iberian shelf – slope region, *Journal of Marine Systems*, Vol. 53 - 74

Villareal, M., Otero, P., Cobas, M., Conde, P. & Almeida, M., 2008, Variability of the circulation off northern and northwestern Iberia, insights from a forecast model, XI International symposium on the Bay of Biscay oceanography, 02-04/04/2008

Sites and catalogues:

<http://amsglossary.allenpress.com/glossary/browse>

http://www.legos.obs-mip.fr/en/share/soa/cgi/getarc/v0.0/index.pl.cgi?contexte=SOA&donnees=maree&produit=modele_fes

www.meteo.ist.utl.pt

www.mohid.com

www.mohid.com/wiki

N.Etopo Bathymetry. Product information catalogue (1988),

see also <http://www.ngdc.noaa.gov/mgg/global/seltopo.html>

<http://oceancurrents.rsmas.miami.edu/atlantic/portugal.html>